Deciphering the influence of evolutionary legacy and functional constraints on the patella: a case study in modern perissodactyls (#96991)

First submission

Guidance from your Editor

Please submit by **14 Mar 2024** for the benefit of the authors (and your token reward) .

✓ **Structure and Criteria**
Please read the 'Structure and Criteria' page for general guidance.

⊞ **Raw data check**
Review the raw data.

🖼 **Image check**
Check that figures and images have not been inappropriately manipulated.

If this article is published your review will be made public. You can choose whether to sign your review. If uploading a PDF please remove any identifiable information (if you want to remain anonymous).

Files

Download and review all files from the materials page.

14 Figure file(s)
5 Table file(s)
1 Raw data file(s)

Structure and Criteria

Structure your review

The review form is divided into 5 sections. Please consider these when composing your review:

1. **BASIC REPORTING**
2. **EXPERIMENTAL DESIGN**
3. **VALIDITY OF THE FINDINGS**
4. General comments
5. Confidential notes to the editor

📄 You can also annotate this PDF and upload it as part of your review

When ready [submit online](#).

Editorial Criteria

Use these criteria points to structure your review. The full detailed editorial criteria is on your [guidance page](#).

BASIC REPORTING

- Clear, unambiguous, professional English language used throughout.
- Intro & background to show context. Literature well referenced & relevant.
- Structure conforms to [PeerJ standards](#), discipline norm, or improved for clarity.
- Figures are relevant, high quality, well labelled & described.
- Raw data supplied (see [PeerJ policy](#)).

EXPERIMENTAL DESIGN

- Original primary research within [Scope of the journal](#).
- Research question well defined, relevant & meaningful. It is stated how the research fills an identified knowledge gap.
- Rigorous investigation performed to a high technical & ethical standard.
- Methods described with sufficient detail & information to replicate.

VALIDITY OF THE FINDINGS

- Impact and novelty not assessed. *Meaningful* replication encouraged where rationale & benefit to literature is clearly stated.
- All underlying data have been provided; they are robust, statistically sound, & controlled.

- Conclusions are well stated, linked to original research question & limited to supporting results.

Standout reviewing tips

The best reviewers use these techniques

Tip	Example
Support criticisms with evidence from the text or from other sources	*Smith et al (J of Methodology, 2005, V3, pp 123) have shown that the analysis you use in Lines 241-250 is not the most appropriate for this situation. Please explain why you used this method.*
Give specific suggestions on how to improve the manuscript	*Your introduction needs more detail. I suggest that you improve the description at lines 57- 86 to provide more justification for your study (specifically, you should expand upon the knowledge gap being filled).*
Comment on language and grammar issues	*The English language should be improved to ensure that an international audience can clearly understand your text. Some examples where the language could be improved include lines 23, 77, 121, 128 – the current phrasing makes comprehension difficult. I suggest you have a colleague who is proficient in English and familiar with the subject matter review your manuscript, or contact a professional editing service.*
Organize by importance of the issues, and number your points	*1. Your most important issue* *2. The next most important item* *3. ...* *4. The least important points*
Please provide constructive criticism, and avoid personal opinions	*I thank you for providing the raw data, however your supplemental files need more descriptive metadata identifiers to be useful to future readers. Although your results are compelling, the data analysis should be improved in the following ways: AA, BB, CC*
Comment on strengths (as well as weaknesses) of the manuscript	*I commend the authors for their extensive data set, compiled over many years of detailed fieldwork. In addition, the manuscript is clearly written in professional, unambiguous language. If there is a weakness, it is in the statistical analysis (as I have noted above) which should be improved upon before Acceptance.*

Deciphering the influence of evolutionary legacy and functional constraints on the patella: a case study in modern perissodactyls

Christophe Mallet [Corresp., 1, 2], **Alexandra Houssaye** [3]

[1] Faculty of Engineering, University of Mons, Department of Geology and Applied Geology, Mons, Belgium

[2] Institute of Natural Sciences, Operational Directorate Earth and History of Life, Brussels, Belgium

[3] Muséum National d'Histoire Naturelle, Mécanismes adaptatifs et évolution (MECADEV), UMR 7179, MNHN, CNRS, Paris, France

Corresponding Author: Christophe Mallet
Email address: christophe.mallet@edu.mnhn.fr

In mammals, the patella is the biggest sesamoid bone of the skeleton and is of crucial importance in posture and locomotion, ensuring the role of a pulley for leg extensors while protecting and stabilizing the knee joint. Despite its central biomechanical role, the relation between the shape of the patella and functional factors, such as body mass or locomotor habit, in the light of evolutionary legacy are poorly known. Here, we propose a morphofunctional investigation of the shape variation of the patella among modern perissodactyls, an order displaying a broad range of body plan, body mass and locomotor habits, to understand how the shape of this sesamoid bone varies between species. Our investigation, relying on three dimensional geometric morphometrics and comparative analyses, reveals that, both within and between the three perissodactyl families (rhinoceroses, equids, tapirs), the patellar shape is more conservative than initially expected. Within families, especially Rhinocerotidae, the shape of the patella strongly follows the phylogenetic affinities rather than variations in body mass. Ontogeny has an impact on the shape as well, being more homogeneous between subadult individuals than between adults. The development of a medial angle, engendering a strong mediolateral asymmetry of the patella, appears convergent in rhinoceroses and equids, while tapirs retain a symmetric bone close to the plesiomorphic condition of the order. This asymmetric patella is likely associated with the presence of a "knee locking" mechanism in both equids and rhinos. The emergence of this condition may be related to a shared locomotor habit (transverse gallop) in both groups. Our investigation underlines unexcepted evolutionary constraints on the shape of a sesamoid bone usually considered as mostly driven by functional factors.

1 **Deciphering the influence of evolutionary legacy and**

2 **functional constraints on the patella: a case study in**

3 **modern perissodactyls**

4

5 Christophe Mallet[1,2], Alexandra Houssaye[3]

6 [1] Operational Directorate Earth and History of Life, Institute of Natural Sciences, Brussels, Belgium

7 [2] Department of Geology and Applied Geology, Faculty of Engineering, University of Mons, Mons,
8 Belgium

9 [3] Mécanismes adaptatifs et évolution (MECADEV), UMR 7179, MNHN, CNRS, Paris, France

10

11 Corresponding author:

12 Christophe Mallet

13 Institute of Natural Sciences, Operational Directorate Earth and History of Life

14 Rue Vautier, 29

15 1000, Brussels

16 Belgium

17

18 Email address: cmallet@naturalsciences.be

19

Abstract

In mammals, the patella is the biggest sesamoid bone of the skeleton and is of crucial importance in posture and locomotion, ensuring the role of a pulley for leg extensors while protecting and stabilizing the knee joint. Despite its central biomechanical role, the relation between the shape of the patella and functional factors, such as body mass or locomotor habit, in the light of evolutionary legacy are poorly known. Here, we propose a morphofunctional investigation of the shape variation of the patella among modern perissodactyls, an order displaying a broad range of body plan, body mass and locomotor habits, to understand how the shape of this sesamoid bone varies between species. Our investigation, relying on three dimensional geometric morphometrics and comparative analyses, reveals that, both within and between the three perissodactyl families (rhinoceroses, equids, tapirs), the patellar shape is more conservative than initially expected. Within families, especially Rhinocerotidae, the shape of the patella strongly follows the phylogenetic affinities rather than variations in body mass. Ontogeny has an impact on the shape as well, being more homogeneous between subadult individuals than between adults. The development of a medial angle, engendering a strong mediolateral asymmetry of the patella, appears convergent in rhinoceroses and equids, while tapirs retain a symmetric bone close to the plesiomorphic condition of the order. This asymmetric patella is likely associated with the presence of a "knee locking" mechanism in both equids and rhinos. The emergence of this condition may be related to a shared locomotor habit (transverse gallop) in both groups. Our investigation underlines unexcepted evolutionary constraints on the shape of a sesamoid bone usually considered as mostly driven by functional factors.

Introduction

In vertebrates, the shape of the skeleton is strongly influenced by different factors like structural, functional, developmental constraints, and evolutionary legacy (Seilacher, 1970, 1991; Gould, 2002). Limb bones, which fulfil various essential functions like body support and locomotion in quadrupeds, are particularly influenced by functional constraints. Variations of body plan, body mass or locomotor habits are indeed known to induce changes in the shape of limb elements (Hildebrand, 1974; Polly, 2007; Biewener & Patek, 2018), as it has been observed in the limb long bones of many clades of tetrapods (see for example Fabre et al., 2013; MacLaren & Nauwelaerts, 2016; Etienne et al., 2020a; Serio, Raia & Meloro, 2020). However, this intense exploration of form-function relationships focused mainly on limb long bones, smaller elements like sesamoid bones remaining poorly studied. Sesamoids are small concentrations of bone generally embedded in dense connective tissue such as tendons or ligaments. They are assumed to increase leverage for muscles and tendons attached to them, while protecting the joints with which they are associated (Vickaryous & Olson, 2008). The emergence of sesamoids in some joints is considered as directly linked to variations in mechanical loads, making them likely to carry a strong functional signal (Vickaryous & Olson, 2008; Eyal et al., 2019).

The patella is the biggest sesamoid bone of the skeleton (Samuels, Regnault & Hutchinson, 2017). Long considered to form within the distal quadriceps tendon, recent findings proved that the patella arises as a bony process at the anterodistal surface of the femur (Eyal et al., 2015, 2019). The patella is later embedded into the quadriceps tendon and articulates with the femur by sliding onto the distal trochlear groove. Onto the patella attach the different ends of the *m. quadriceps* as well as the *m. gluteobiceps*, all being powerful knee extensors (Barone, 2010a; Samuels, Regnault & Hutchinson, 2017; Etienne, Houssaye & Hutchinson, 2021) (Figure 1). The patella is also connected to the tibia through the patellar tendon, and additional lateral and medial tendons (Barone, 2010a; Samuels, Regnault & Hutchinson, 2017). The main functional role of the patella is to modify the lever arm of the *m. quadriceps*. By moving the quadriceps tendon away from the centre of rotation of the knee joint, the patella acts as a pulley and reduces the muscular energy required to extend the leg, while increasing the velocity of the rotation (Aglietti & Menchetti, 1995; Allen et al., 2017). In mammals, the patella also centralizes the forces coming from the four heads of the *m. quadriceps* into a single point of application and transmits them without friction to the tibial tuberosity. In addition, the patella acts as a protective element for the knee joint (Aglietti & Menchetti, 1995).

Given all these complementary functional roles, the patella therefore constitutes a crucial part of the knee and of the hindlimb as a whole. This functional importance led to various works that explored the biomechanical involvement of the patella in the hindlimb movements and its mechanical advantage, mostly in humans and related hominoids (Bizarro, 1921; Ellis et al., 1980; Aglietti & Menchetti, 1995; Lovejoy, 2007; Dan et al., 2018; Pina et al., 2020; Schneider, Rooks & Besier, 2022). These aspects have been rarely addressed in other groups of amniotes (Alexander & Dimery, 1985; Chadwick et al., 2014; Allen et al., 2017), most of the studies focusing more on the evolutionary relevance of the presence or absence of the patella (Jerez, Mangione & Abdala, 2010; Ponssa, Goldberg & Abdala, 2010; Corina Vera, Laura Ponssa & Abdala, 2015; Abdala, Vera & Ponssa, 2017; Samuels, Regnault & Hutchinson, 2017). While the inner bony structure of the patella has sometimes been explored in regards to functional constraints (Raux et al., 1975; Toumi et al., 2006; Houssaye, Perthuis & Houée, 2021), the variation of its external shape, considered as relatively conservative in amniotes (Samuels, Regnault & Hutchinson,

81 2017), remains largely understudied. Only a few studies tried to investigate the form-function
82 relationships at a larger interspecific scale, mostly in mammals (Valois, 1917; Raymond & Prothero,
83 2012; Pina et al., 2020; Garnoeva, 2022). Therefore, the variation of the shape of the patella in relation
84 with functional constraints remains virtually unknown in amniotes.

85 In this context, we chose to explore the shape variation of the patella in modern perissodactyls (within and
86 between rhinoceroses, equids, and tapirs), and to investigate its relations with functional (body mass,
87 locomotor habit) factors within a phylogenetically informed framework. The order Perissodactyla, despite
88 a limited number of living species, presents a diversity of body mass, body plan, ecological affinities and
89 locomotor habits that make this group well suited for a morphofunctional investigation of the patella.
90 Modern rhinoceroses inhabit various environments from open savannas to dense rainforests, associated
91 with diverse feeding strategies, from specialized grazers to generalist browsers (Dinerstein, 2011). These
92 three-toed animals constitute the second heaviest land mammal group after elephants (Alexander & Pond,
93 1992), and contrary to them, show great variations of body mass (BM) among the five living species:
94 from 600 for *Dicerorhinus sumatrensis* (Fischer, 1814) up to 3,500 kg for *Ceratotherium simum*
95 (Burchell, 1817). Body mass in rhinos can vary strongly between males and females in some species
96 (Zschokke & Baur, 2002; Dinerstein, 2011), as well as their body plan, from long-legged black rhino
97 *Diceros bicornis* to short-legged white rhino *C. simum*. This diversity of body construction and ecological
98 preferences makes them a particularly well-suited group for studying the link between patellar shape and
99 functional factors. Modern perissodactyls also comprise seven species of equids and four of tapirs. These
100 two clades show less intragroup variations of size and body plan. Tapirs are forest-dwellers weighting up
101 to 400 kg (Medici, 2011) and retaining some plesiomorphic characters of the order Perissodactyla in their
102 limbs, such as a tetradactyl manus and a tridactyl pes (MacLaren & Nauwelaerts, 2016, 2017). At the
103 opposite, equids, weighting up to 600 kg, show a highly derived limb structure adapted for running and
104 living in open habitats, with monodactyl manus and pes (Rubenstein, 2011). These three families also
105 show a gradient of stature and proportions in their limb construction, from cursorial equids to
106 "mediportal" tapirs and graviportal rhinos, likely to be associated with differences in patellar shape
107 (Eisenmann & Guérin, 1984). Recent advances in functional morphology underlined how body mass
108 could drive – or not – the shape of limb bones in perissodactyls (MacLaren & Nauwelaerts, 2016, 2017;
109 Hanot et al., 2017, 2018; MacLaren et al., 2018; Mallet et al., 2019, 2020, 2021, 2022; Etienne et al.,
110 2020b), but without consideration for the patella.

111 Moreover, some perissodactyls (equids and rhinoceroses) are known to possess a "knee locking"
112 mechanism in their hindlimb: they are able to lock the patella and the medial patellar tendon above the
113 medial trochlear ridge of the distal femur (Hermanson & MacFadden, 1996; Schuurman, Kersten &
114 Weijs, 2003). Doing so, the natural flexion of the limb that could be engendered in relation with body
115 weight becomes impossible, allowing to save muscular energy for long periods of standing. Long
116 considered as passive, *in vivo* experiments demonstrated that this mechanism does require muscular
117 energy, even though far much less than would be needed without this apparatus (Schuurman, Kersten &
118 Weijs, 2003). Broadly studied in domestic equids for veterinary purposes, this locking mechanism is less
119 documented *in vivo* in rhinos and only inferred through the shape of the distal femur but not directly
120 through that of the patella (Shockey et al., 2008; Danaher, Shockey & Mihlbachler, 2009; Janis et al.,
121 2012; Mihlbachler et al., 2014). A recent investigation on the microanatomy of the patella in modern
122 perissodactyls highlighted microanatomical changes related to different functional factors, notably the
123 presence of the knee locking mechanism (Houssaye, Perthuis & Houée, 2021). But a similar comparative

124   investigation remains to be conducted for deciphering how functional factors are related to the external
125   shape of the patella in this group.

126   For all these reasons, we chose to explore both intra- and interspecific variation of the shape of the patella
127   among modern rhinoceroses, and to compare it with tapirs' and equids', in order to shed light on how this
128   crucial sesamoid bone is influenced by functional constraints and evolutionary legacy among
129   Perissodactyla. We relied on a 3D geometric morphometrics approach to investigate the form-function
130   relationships on the patella. Given previous results on the shape variation of hindlimb long bones (Mallet
131   et al., 2019, 2020) and on the inner structure of the patella (Houssaye, Perthuis & Houée, 2021) in modern
132   rhinos, we hypothesize: (1) higher interspecific than intraspecific variation of the shape of the patella in
133   rhinos; (2) a main influence of body mass on interspecific variation despite strong phylogenetic affinities;
134   (3) more marked differences between rhinos and tapirs than between rhinos and equids, given the shared
135   presence of a knee locking mechanism (Schuurman, Kersten & Weijs, 2003; Shockey et al., 2008); (4)
136   this mechanism being nevertheless associated with shape differences in these two latter groups given the
137   differences in body plan, body mass, locomotor habits and phylogenetic affinities.

Material and Methods

Studied sample

We selected a sample composed of 65 patellae of modern perissodactyls housed in eight institutions (American Museum of Natural History, New York, USA; Powell Cotton Museum, Birchington-on-Sea, UK; Idaho Museum of Natural History, Pocatello, USA; Muséum National d'Histoire Naturelle, Paris, France; Museum of Vertebrate Zoology, Berkeley, USA; Natural History Museum, London, UK; NMB: Naturhistorisches Museum Basel, Basel, Switzerland; Institute of Natural Sciences, Brussels, Belgium) and representing the five modern species of rhinos (38 patellae), together with four modern species of tapirs (12 patellae) and 7 species (9 subspecies) of modern equids (15 patellae) (Table 1, Figure 2). The sample includes 29 males, 17 females and 19 specimens without sex attribution. It involves 50 adults, 13 subadults or juveniles and 2 specimens of unknown age (see Table 1 for details). Because of the higher intrafamilial diversity of rhinos, we chose to focus first on this group. We performed our analyses successively on three subsamples: a) adult rhinoceroses only, b) all rhinos including young specimens, and c) all rhinos, equids, and tapirs. All anatomical terms follow classic anatomical and veterinary works (Federative Committee on Anatomical Terminology, 1998; Barone, 2010b), and are given in Figure 3.

3D models

Patellae were mostly digitized using a structured-light three dimensional scanner (Artec Eva) and reconstructed with Artec Studio professional (v12.1.1.12 – Artec 3D, 2018). Twelve specimens were scanned using a Creaform HandySCAN 300 laser surface scanner and reconstruted using the VX Models software (Creaform, USA). Nine patellae were scanned using high-resolution computed tomography at the micro-CT laboratory of the Natural History Museum, London, UK (Nikon HMX 225 ST system), and six at the AST-RX platform at the Muséum National d'Histoire Naturelle, Paris (UMS 2700; GE phoenix|X-ray v|tome|xs 240), with reconstructions performed using the CT-agent software (Nikon Metrology, Leuven, Belgium), and DATOX/RES software (phoenix datos|x). Bone surfaces were extracted as meshes using Avizo 9.4 (Thermo Fisher Scientific, 2018). Three specimens were retrieved on the online deposit MorphoSource (see Table 1 for details). Only right bones were selected for digitization; when unavailable, we selected left bones instead and mirrored the 3D models before analysis using MeshLab (v2022.02 – Cignoni et al., 2008). ARK identifiers of each 3D model are provided in Supplementary Table T1.

3D geometric morphometrics

We analysed the shape variation of our sample using a 3D geometric morphometrics approach. This widely used methodology allows to quantify and visualize the morphological differences between objects by comparing the spatial coordinates of landmarks placed on them (Adams, Rohlf & Slice, 2004; Zelditch et al., 2012; Mitteroecker & Schaefer, 2022). The shape of the patella was quantified by placing a set of anatomical landmarks and curve and sliding semi-landmarks on the meshes, as described by Gunz, Mitteroecker, & Bookstein (2005) and Botton-Divet et al. (2016). Anatomical landmarks and curves were placed on meshes using the IDAV Landmark software (v3.0 – Wiley et al., 2005). We defined 6 anatomical landmarks associated with 2 curves allowing to cover the shape diversity of the patella in modern perissodactyls (Figure 3). We evaluated the relevance of these anatomical landmarks to describe the shape by conducting repeatability tests. We considered three specimens of *Ds. sumatrensis* chosen to display the closest morphology. We successively digitized ten times the anatomical landmarks on the

179   three specimens to obtain thirty replications of the landmark datasets. We superimposed these landmark
180   configurations using a Generalized Procrustes Analysis (GPA, see below) then performed a Principal
181   Component Analysis (PCA) to visualise the placement of each repeated set of measurement relatively to
182   each other. It appeared clearly that the variation within specimens was lower than between specimens,
183   confirming the relevance of our landmarks to precisely describe the shape variation (see Supplementary
184   Figure S1).

185   Anatomical landmarks and curve sliding semi-landmarks were placed on each specimen. A template was
186   created for the placement of the surface sliding semi-landmark on each patella. A specimen (*C. simum*
187   AMNH M-51854) was selected as the initial specimen on which all anatomical landmarks, curve and
188   surface sliding semi-landmarks were placed. This specimen was selected for its average shape and size
189   allowing to ensure the correct placement of the landmarks on all the other specimens despite the great
190   variation of size and shape in the sample. It was then used as a template for the projection of surface
191   sliding semi-landmarks on the surface of all other specimens. Projection was followed by a relaxation step
192   ensuring that projected points matched the surface of the meshes. Curve and surface semi-landmarks were
193   then slid by minimizing the bending energy of a thin plate spline (TPS) between each specimen and the
194   template at first, then four times between the result of the previous step and the Procrustes consensus of
195   the complete dataset (see Gunz, Mitteroecker & Bookstein, 2005; Botton-Divet et al., 2016 for details
196   regarding this process). Once this process achieved, all landmarks could be treated as geometrically
197   homologous. We then performed a Generalized Procrustes Analysis (GPA) to remove the effect of
198   relative size, location and orientation of the different landmark conformations (Gower, 1975; Rohlf &
199   Slice, 1990). Projection, relaxation, sliding processes and GPA were conducted using the "Morpho"
200   package (v2.10 – Schlager, 2017) in the R environment (v4.2.1 – R Core Team, 2014).

201   Superimposed conformations of landmarks were then used to compute a PCA in order to reduce
202   dimensionality (Gunz & Mitteroecker, 2013). PC scores where then used to compute Neighbour-Joining
203   (NJ) trees and morphospaces allowing to visualise the distribution of each individual relatively to each
204   other. To visualise how shape varies in association with the specimen distribution, we computed
205   theoretical shapes associated with both minimal and maximal values for the two first PCs using a TPS
206   deformation of a template mesh. To emphasize the location of the main shape changes on the patella
207   among the sample, we displayed the vectors of displacement between all landmarks of the two theoretical
208   shapes using the "rgl" package (v0.109.6 – Adler & Murdoch, 2020). As described by Botton-Divet
209   (2017) and Pintore *et al.* (2021), we applied a gradient of colour to these segments according to their
210   distance to highlight which parts varied the most, these segments being displayed directly onto the
211   superimposed theoretical shapes.

212   We explored the relation between shape and specific attribution, sex, age class and size (see below).
213   Permutational analyses of variance (PERMANOVAs) were performed on PC scores against the specific
214   attribution and in interaction with the sex (and in addition with the age class for our second subsample
215   including subadult rhinos) to test for the impact of these parameters on the patellar shape. We explored
216   allometric variation (i.e., shape variation linked to size; Hallgrímsson et al. 2009; Zelditch et al. 2012;
217   Mitteroecker et al. 2013; Klingenberg 2016) within our sample using different approaches. Pearson's
218   correlation tests were performed to test for correlation between the scores of the two first PC and the
219   centroid size of the specimens. We performed a Procrustes ANOVA (a linear regression model using
220   Procrustes distances between species instead of covariance matrices – Goodall 1991; Adams &
221   Otárola-Castillo 2013) to quantify the shape variation related to the centroid size taking into account

222   species attribution to highlight respective roles of centroid size and specific determination on the global
223   shape variation. This set of analyses (PERMANOVA, Pearson's correlation tests, Procrustes ANOVAs)
224   was applied respectively on the three subsamples described above. Detailed NJ trees and PCA plots for
225   equids and tapirs only are provided as Supplementary Data.

Proxies of body mass

227   In the absence of most of the mass values of the specimens constituting our sample, we chose two proxies
228   of body mass: 1) the centroid size (CS) of each patella, generally used to address allometric variation,
229   defined as the square root of the sum of the square of the distance of each point to the centroid of the
230   landmark set (Zelditch et al., 2012); it is generally considered as a good proxy of the body mass of the
231   animal ; and 2) the minimal femoral circumference (FC) of each specimen, a measurement classically
232   used in equations of body mass estimation. Indeed, the femur being a crucial bone for weight support in
233   quadrupeds, its circumference is known to strongly covary with body mass (Anderson, Hall-Martin &
234   Russell, 1985; Scott, 1990; Damuth & MacFadden, 1990; Campione & Evans, 2012; Campione, 2017).
235   FC therefore provides a proxy of mass relatively independent of the patella itself.

Phylogenetic framework

237   To test the presence of a phylogenetic signal in our shape data, we constructed a composite cladogram
238   using trees previously computed on molecular data and craniodental and postcranial characters (Figure 2).
239   Branch relations, lengths and occurrence dates were retrieved and merged following phylogenetic
240   reconstructions proposed in recent works (Steiner & Ryder, 2011; MacLaren et al., 2018; Bai et al., 2020;
241   Cirilli et al., 2021; Antoine et al., 2021; Liu et al., 2021; Pandolfi et al., 2021). The phylogenetic relation
242   of *Ds. sumatrensis* relatively to the other modern species has long been debated (see Mallet et al., 2019).
243   As recent works based on molecular and morphological data agreed on the phylogenetic position of this
244   species (Antoine et al., 2021; Liu et al., 2021; Pandolfi et al., 2021), we considered here *Ds. sumatrensis*
245   as sister taxon of the *Rhinoceros* genus.

246   We addressed the effect of phylogenetic signal on shape and centroid size in our dataset. Given the small
247   numbers of rhino species (five) on the two first subsamples, tests for phylogenetic signal were only
248   performed on the third subsample, containing all perissodactyl species. For species represented by several
249   specimens, we computed species mean shapes (Botton-Divet et al., 2017; Serio, Raia & Meloro, 2020;
250   Mallet et al., 2021, 2022). We computed a first GPA with all specimens of the third subsample (all
251   perissodactyls) as described previously, then we computed the Procrustes consensus (or mean shape) of
252   each species in this geometric space. These Procrustes consensuses were superimposed in a second GPA
253   before computing a new PCA. We then addressed the effect of phylogeny on mean centroid sizes per
254   species with the univariate K statistic (Blomberg et al., 2003), using the function "phylosig" in the
255   "phytools" package (Revell, 2012). We also addressed the effect of phylogenetic relationships on shape
256   data using the multivariate K statistic (K_{mult}) on PC scores (Adams, 2014). K_{mult} index allows the
257   comparison between the rate of observed morphological change and that expected under a Brownian
258   motion on a given phylogeny (Blomberg et al., 2003; Adams, 2014). K_{mult} was computed using the
259   function "physignal" in the "geomorph" package (v4.0.4 – Adams & Otárola-Castillo, 2013).

260   All statistic tests were considered as significant for p values ≤ 0.01. However, as we agree with the recent
261   works calling for a continuous approach of the p value (Wasserstein, Schirm & Lazar, 2019; Ho et al.,
262   2019), we chose to mention and comment results having a p value up to 0.05 as well.

263 **Results**

264 <u>Shape variation in adult rhinoceroses</u>

265 The distribution of the specimens both in the NJ tree and in the morphospace shows a clear distinction
266 between African and Asiatic rhinos. Along the NJ tree (Figure 4), specimens of *C. simum* and *Dc.*
267 *bicornis* plot together and oppose to *Ds. sumatrensis*, *R. sondaicus* and *R. unicornis*. The *Dc. bicornis* and
268 *C. simum* specimens are mixed, as are the *R. sondaicus* and *R. unicornis* specimens. Those of *Ds.*
269 *sumatrensis* form an isolated and homogeneous cluster. The morphospace of the first two axes of the
270 PCA, representing 47.6%, displays a similar structure (Figure 5A). PC1, which carries 34.3% of the
271 global variance, separates African rhinos towards negative values from Asiatic rhinos towards positive
272 values. *C. simum*, occupies the highest negative values of the axis while *R. unicornis* and *R. sondaicus*
273 occupy the highest positive values. *Ds. sumatrensis* specimens poorly overlap the genus *Rhinoceros* along
274 the PC1. PC2 represents 13.4% of the variance and is mainly driven by the isolation of *Ds. sumatrensis*
275 towards the positive values, while all other species overlap around null and negative values.

276 A Pearson's correlation test indicates that PC1 is marginally correlated (r = -0.36; p = 0.06), whereas PC2
277 is highly correlated (r = -0.53; p < 0.01) with the centroid size. The PERMANOVA of PC scores against
278 the specific attribution and in interaction with the sex of the specimen confirms a highly significant
279 correlation between the shape of the patella and the specific attribution (R^2 = 0.53; p < 0.01). The sex
280 attribution alone is not significantly correlated with the shape (p = 0.36), while its interaction with
281 specific attribution is marginally not significantly correlated with shape data (R^2 = 0.13; p = 0.07).

282 Shape variation along PC1 is mainly related to the proximodistal extension of the base and the aspect of
283 the medial angle (Figure 5B-a). Towards minimal values, patella display a rounded and smooth general
284 aspect. The articular surface for the femur is regularly concave and has a regularly convex cranial surface.
285 The proximal end of the medial articular surface poorly exceeds that of the lateral articular surface. The
286 medial ridge is regularly sigmoid in medial view, with a more rounded distal part. The base is
287 mediolaterally broad and extends poorly proximally, being only slightly higher than the proximal border
288 of the articular surface. The medial angle is rounded and smooth, pointing mediodistally. Towards
289 maximal values, the patella has a more angular general aspect. The cranial surface of the patella forms a
290 relatively straight dorsoventral line, before displaying a caudoventral inflexion towards the apex. The
291 proximal end of the medial articular surface exceeds greatly that of the lateral articular surface. The
292 medial ridge is straight in medial view, forming a shallow relief caudally to the apex. The base forms a
293 saliant and regular triangle with a relatively narrow base, and a right angle markedly higher than the
294 proximal border of the articular surface. The medial angle forms a regularly rounded protrusion pointing
295 strictly medially.

296 Shape variation along PC2 is mainly dominated by changes in the antero-posterior broadness of the
297 patella, the proximodistal extension of the base and the apex, and the aspect of the medial angle (Figure
298 5B-b). Towards minimal values, the patella has a robust general aspect, especially antero-posteriorly, with
299 a base extending strongly dorsally. The articular surface for the femur has an irregular shape pointing in
300 proximal direction. In medial view, the anterior surface of the patella follows a straight line from the base
301 before forming a marked obtuse angle towards the apex. The proximal end of the medial articular surface
302 exceeds markedly that of the lateral articular surface. The medial ridge is poorly concave, almost straight,
303 in medial view. The base is thick, broadly triangular and forms a saliant proximal protrusion. The medial

304 angle forms a broad triangle pointing directly medially. The apex is thick and short. Towards maximal
305 values, the patella is flatter antero-posteriorly, with a prominent protrusion of the apex. The articular
306 surface for the femur has an irregular triangular shape pointing distally. The anterior surface of the patella
307 forms a regular convex surface from the base to the apex. The proximal end of the medial articular
308 surface poorly exceeds that of the lateral articular surface. The medial ridge is regularly concave in
309 medial view and forms a convex relief above the apex. The base is very short and poorly extended
310 proximally. The medial angle forms a large, rounded protrusion pointing medially. The apex expands
311 largely and forms a regular saliant relief directed posterodistally.

312 The regression plot of the Procrustes ANOVA performed on shape against log centroid size shows a
313 rather important spreading of the specimens around the regression line (Figure 6A). Towards maximal CS
314 values, *C. simum* opposes clearly to *R. unicornis* on each side of the line, while specimens of *Ds.*
315 *sumatrensis* show a relatively good fit to the line. Specimens of *Dc. bicornis* and *R. sondaicus* spread
316 both above and below the line and their position remains hard to interpret (both being adult males likely
317 to show an unusual shape). Shape variation associated with centroid size mainly involves changes in the
318 general proportions of the patella, as well as the relative development of the base, the medial angle and, at
319 a lesser extent, the apex (Figure 6A and 6B). Towards high values of centroid size, the patella broadens
320 antero-posteriorly, showing a more rounded and smooth general aspect. The base is broad and thick,
321 poorly developed proximally, forming a convex relief posteriorly to the articular surface. The medial
322 angle forms a smooth triangle pointing medially, distally, and posteriorly. The apex appears short and
323 broad.

324 Moreover, the shape is significantly correlated with both centroid size and specific affiliation ($p < 0.01$)
325 (Table 2). However, while centroid size accounts for 11% of the global variance, specific attribution
326 accounts for almost half of the total variance (44%). Interaction between centroid size and specific
327 attribution is not significant ($p = 0.60$). In accordance with the strong correlation between centroid size
328 and femoral circumference (Pearson's correlation test; $r = 0.75$, $p < 0.01$), very similar results are
329 obtained when considering the log of the minimal femoral circumference instead of the centroid size in
330 the Procrustes ANOVA (Table 2). The regression plot highlights a signal strongly driven by *Ds.*
331 *sumatrensis* and one specimen of *R. unicornis*. When removing these two species from the Procrustes
332 ANOVA, the correlation between shape data and size is not significant anymore ($p = 0.18$), while the
333 correlation between size and specific attribution remains strong and significant ($R^2 = 0.44$, $p < 0.01$).

334 <u>Ontogenetic variation in rhinoceroses</u>

335 The addition of the subadult rhinoceroses to the sample (three *C. simum*, two *Dc. bicornis*, three *R.*
336 *sondaicus*, one *R. unicornis* and one *Ds. sumatrensis*) does not strongly modify neither the general
337 repartition of the specimens in the NJ tree nor the morphospace (Figure 7A and 7B). The different species
338 are however not as well distinguished as previously observed in the first subsample, with two *R.*
339 *sondaicus* plotting respectively with *Dc. bicornis* and *Ds. sumatrensis*, and one *C. simum* plotting with
340 *Dc. bicornis* and more overlaps on the PC1 and 2. The global dispersion of species drastically increases,
341 especially for *R. sondaicus*. Most subadult specimens occupy a relatively central position in the
342 morphospace and plot close to each other. PC1 and centroid size remain correlated ($r = -0.35$; $p = 0.02$)
343 while PC2 is not correlated anymore with CS ($p = 0.48$). The PERMANOVA of PC scores against the
344 specific attribution and in interaction with the age of the specimen indicates a high correlation between
345 the shape and the specific attribution ($R^2 = 0.41$; $p < 0.01$), although weaker than for adults only. Shape

346 variation along PC1 and PC2 within this subsample is highly similar to the one observed for adult rhinos
347 alone and is detailed in Supplementary Figure S2.

348 The results of the Procrustes ANOVA are very similar to what was observed for adult specimens only.
349 The regression plot of shape against log centroid size shows no major difference with the one obtained for
350 adult rhinos only and the associated shape variation is very similar to the same variation for adult rhinos
351 (see Supplementary Figure S2 for details). Detailed results of the PERMANOVA and the Procrustes
352 ANOVA for this subsample are available in Supplementary Table T2.

353 <u>All perissodactyls</u>

354 When considering the third subsample (all rhinos, tapirs, and equids), shape data carries a significant but
355 low phylogenetic signal (K_{mult} = 0.143, P < 0.01), while the mean centroid size per species does not carry
356 a significant phylogenetic signal (p = 0.54). The distribution of the specimens both in the NJ tree and in
357 the morphospace strictly separates rhinos, equids, and tapirs (Figure 8). Among rhinos, the repartition
358 previously observed is conserved, with a rather good separation between African and Asiatic rhinos – the
359 only specimens plotting outside of their respective species being the subadults. The separation between
360 species is far less clear among tapirs. All specimens of *Tapirus indicus*, the largest and only Asiatic
361 species of tapir, plot together, while the other three species are mixed. When considered separately, the
362 different tapir species discriminate well on the PCA but stay mixed on the NJ tree (see Supplementary
363 Figure S3). Among equids, most *E. quagga* plot together, as do most donkeys (*E. africanus asinus*, *E.*
364 *hemionus*), far from *E. quagga*. Between them, *E. grevyi* plot together with horses (*E. ferus caballus* and
365 *E. ferus przewalskii*). Two larger specimens of *E. asinus* are mixed among horses and quaggas,
366 respectively. When considered alone, equids show a strong mixing, despite most zebras and horses
367 grouping together, respectively (see Supplementary Figure S4).

368 The morphospace of the first two axes of the PCA, representing 63.3%, is structured by a strict separation
369 between the three main perissodactyl families, the separation between species within each family being
370 poorly visible (Figure 9A). PC1 carries 40.4% of the global variance and clearly separates rhinos and
371 equids in the negative part of the axis from tapirs in the positive part. All equids group together with no
372 clear structure, except for *E. hemionus*, plotting far away from the equid cluster. Among each family, the
373 separation between species is far less clear. Rhinos, to the exclusion of *Ds. sumatrensis* and to *C. simum*,
374 although to a lesser extent, plot together with almost all equids. Among tapirs, only *T. pinchaque* isolates
375 slightly from other species. Along PC2, which accounts for 22.9% of the variance, rhinos, and tapirs in
376 the negative part of the axis are clearly separated from equids in the positive part.

377 PC1 and PC2 are both highly correlated with the centroid size (Pearson's correlation test: r = -0.68; p <
378 0.01 and r = -0.39; p < 0.01, respectively). PERMANOVA confirms an extremely high and significant
379 correlation between the shape of the patella and the specific attribution (R^2 = 0.77; p < 0.01). Conversely,
380 neither sex nor the interaction between specific attribution and sex are significantly correlated with shape
381 data.

382 Shape variation along PC1 is mainly related to the degree of asymmetry of the patella, the development of
383 the medial angle, and the anteroposterior broadening of the base (Figure 9B-a). Both extreme shapes
384 reflect respectively rhino and tapir morphotypes. Towards minimal values, patellae exhibit a "rhino-like"
385 general aspect. The anterior surface is relatively flat, with a straight anterior border forming a well-
386 marked angle (around 125°) towards the apex. The articular surface for the femur is globally rounded and

387   smooth. The medial ridge is regularly sigmoid and poorly concave in medial view. The base is broad
388   mediolaterally and extends poorly proximally. The medial angle is rounded and smooth and extends
389   strongly mediodistally. The apex is broad and massive antero-posteriorly, and poorly expands distally.
390   Towards maximal values, the theoretical shape of the patella has a "tapir-like" aspect, is strongly
391   symmetric, with no medial angle. The anterior surface is strongly and regularly curved from the base to
392   the apex. The articular surface for the femur is globally rectangular with symmetric medial and lateral
393   facets. The medial ridge is concave in medial view, the rounded distal part towards the apex protruding
394   only slightly. The base is well-developed and broad antero-posteriorly, ending in a marked knob pointing
395   medio-proximally. The medial angle is almost absent, reduced to a smooth relief along the medial border
396   of the articular surface. The apex is thin, wedge-shaped, poorly extended distally relatively to the articular
397   surface.

398   Along PC2, shape variation is mainly related to the development and aspect of the base and of the medial
399   angle (Figure 9B-b). Towards minimal values, the shape displays again a "rhino-like" general aspect, but
400   more mediolaterally compressed than on the PC1. The base forms a salient relief extending markedly
401   proximally. The medial angle is rounded, smooth and extends in medial direction. Towards maximal
402   values, patellae display an "equid-like" general aspect, shaped as triangular-based pyramid. The anterior
403   surface is strongly convex, extending strongly anteriorly. In medial view, the anterior border of the patella
404   forms a 45-degrees downward slope towards the apex. The articular surface for the femur forms a marked
405   angle pointing medially. The proximal end of the medial articular surface is situated way below that of the
406   lateral articular surface. The medial ridge forms a smooth sigmoid in medial view, the proximal part
407   overhanging the articular surface in posterior direction. The base expands massively in anterior direction
408   and forms a large flat surface strongly inclined distally towards the medial angle. No marked relief is
409   visible on the surface of the base. The medial angle is broad and rounded, extending strongly medio-
410   distally. The apex is short antero-posteriorly.

411   Shape is significantly correlated with both centroid size (Procrustes ANOVA: $R^2 = 0.23$; $p < 0.01$) and
412   specific affiliation ($R^2 = 0.55$; $p < 0.01$) (Table 3). As for rhinos alone, specific attribution accounts for
413   way more variance than the centroid size itself. The interaction between specific attribution and size is not
414   significantly correlated with shape ($p = 0.64$). Similarly, the femoral circumference among all
415   perissodactyls is extremely correlated to the centroid size of the patella ($r = 0.89$, $p < 0.01$). Consequently,
416   shape is highly correlated with femoral circumference (Procrustes ANOVA: $R^2 = 0.25$; $p < 0.01$) and even
417   more strongly with specific attribution ($R^2 = 0.54$; $p < 0.01$), while the interaction of these two factors is
418   not significantly correlated with shape ($p = 0.53$).

419   The regression plot of shape against log centroid size shows a limited spreading of the specimens around
420   the regression line (Figure 10A). Towards maximal CS values, *C. simum* is now below the regression line
421   while *R. unicornis* and *Ds. sumatrensis* plot above. Once again, the position of the few specimens of *Dc.*
422   *bicornis* and *R. sondaicus* remains hard to interpret. Almost all equids plot above the regression line with
423   few exceptions: one *E. caballus* and two *E. asinus*, one of which being a draught breed with the highest
424   CS value of the sample, and one *E. zebra hartmannae* (a subadult) plotting among tapirs. All tapirs plot
425   together below the regression line and are ordered from the lightest body mass to the heaviest one along
426   the centroid size values. Shape variation associated with centroid size mainly reflects differences between
427   tapirs for minimal values and rhinos for maximal values. Changes in centroid size among perissodactyls
428   involve changes in the general asymmetry of the patella, the relative development of the medial angle and
429   the cranio-caudal broadening of the bone (Figure 10A and 10B).

Discussion

430

431   <u>Intra- and interfamily variation of shape</u>

432   Our results highlight a marked distinction between African and Asiatic rhinos, despite important weight
433   variations within these two groups, suggesting that the shape of the patella among rhinoceroses is highly
434   related to phylogenetic affinities prior to body mass. Each rhino species possesses a unique patellar shape
435   that can hardly be confused with others'. This confirms our first hypothesis that interspecific variation is
436   stronger than intraspecific one for the patellar shape. In the hindlimb, the patella articulates directly with
437   the trochlear groove of the femur, while it is only linked with the tibia by ligaments. Moreover, the patella
438   in mammals is known to individualize from the femur in the early developmental stages of the embryo
439   (Eyal et al., 2015, 2019). The patella and the femur are therefore strongly bonded bones, both on
440   functional and developmental aspects. These results are congruent with previous ones showing that
441   femoral shape variation is also mostly driven by phylogenetic affinities over functional factors such as
442   body mass, especially the distal part directly linked with the patella (Mallet et al., 2019, 2022).

443   Although statistically limited, our results allow to draw preliminary considerations on the relation
444   between the shape of the patella, sex attribution and age class among modern rhinoceroses. Our current
445   data do not allow to detect a clear shape distinction between males and females. The appendicular
446   skeleton of modern rhinos is poorly dimorphic (Guérin, 1980; Mallet et al., 2019) with phenotypic
447   dimorphic traits being generally limited to larger horns or slightly heavier males or females (depending on
448   the species) (Dinerstein, 1991, 2011; Zschokke & Baur, 2002). As seen above, body mass variation seems
449   to affect poorly the patellar shape in rhinos. Our results confirm that the patella as well do not bear a
450   significant dimorphic signal among modern rhinos.

451   Conversely, the inclusion of juvenile and subadults specimens in our sample clearly indicates shape
452   changes of the patella in rhinos along the animal growth, namely ontogenetic allometry (Klingenberg,
453   2016). Subadults for a given species tend to show similarities with lighter rhino species: young *C. simum*
454   resemble adults *Dc. bicornis*, while young *Dc. bicornis* are close to adult *Ds. sumatrensis*. Young
455   individuals also show more similarities between them than between adults. The shape of the patella in
456   young rhinos is therefore relatively homogeneous between the different species, before shapes diverge
457   later in the animal growth. Studies dealing with ontogenetic allometric trajectories of the patella in
458   mammals are extremely scarce. One of the few available case study, dealing with the distal femur of
459   Hominidae (Tallman, 2016), indicates, contrary to our results, a convergence towards a shared knee
460   morphology in adults among Hominidae, while young individuals display very different knee shapes.
461   This ontogenetic convergence, likely linked to the rise of facultative or permanent bipedalism, is the
462   opposite of what we observe in rhinos.

463   Among perissodactyls, the three families (Tapiridae, Equidae, Rhinocerotidae) are clearly distinct, with
464   tapirs differing even more from rhinos than equids. This is in accordance with our third hypothesis,
465   assuming more differences between rhinos and tapirs than between rhinos and equids. This result does not
466   reflect the phylogenetic relationships among the family Perissodactyla, rhinos and tapirs being sister taxa,
467   but rather rely on the shared high development of the medial angle, creating a strong mediolateral
468   asymmetry, absent in tapirs. The patella condition in tapirs is very close to the one observed in early
469   perissodactyls, although this bone is poorly described in literature (Bai et al., 2017), while rhinos and
470   equids show a more derived condition.

471   Furthermore, intrafamily variations reveal to be higher among rhinos than among equids and tapirs. These
472   relative differences in variation within the three families may be related to their respective evolutionary
473   history. Divergences between the different rhino clades occurred from the Oligocene to Miocene (Figure
474   2) (Bai et al., 2020; Antoine et al., 2021; Liu et al., 2021). Tapir branches also diverged during the
475   Miocene (Steiner & Ryder, 2011; MacLaren et al., 2018) but this clade remained monogeneric, contrary
476   to rhinos. Equids, another monogeneric clade, includes species that diverged very recently during the
477   Pliocene (Steiner & Ryder, 2011; Cirilli et al., 2021). The higher genera richness characterizing the
478   family Rhinocerotidae may explain the higher diversity of patellar shape in this clade relatively to its
479   sister groups.

480   Microanatomical investigations on the patella of modern perissodactyls revealed no increase in
481   compactness with body mass and no thickening of the cortex on muscle insertions but on the patellar
482   ligament on the cranial side of the bone (Houssaye, Perthuis & Houée, 2021). These results are consistent
483   with ours on the rather conservative nature of this bone in relation to body mass variation. Conversely, the
484   microanatomy distinguishes more rhinos and equids than rhinos and tapirs, contrary to our results,
485   underlining a decoupling between the external morphology of the patella and its internal structure among
486   perissodactyls.

487   <u>Functional constraints and "knee locking" mechanism</u>

488   In modern rhinoceroses, our results underline a significant relation between the patellar shape and both its
489   size and the femoral circumference, an excellent proxy of body mass in quadrupeds (Scott, 1990;
490   Campione & Evans, 2012; Campione, 2017). The centroid size of the patella therefore appears directly
491   related to body weight in rhinos, as previously observed for long bones and ankle bones in these animals
492   (Mallet et al., 2019; Etienne et al., 2020b). However, shape relation with size is limited, allometry
493   accounting for only 11% of the observed shape variation. The influence of body mass on the patellar
494   shape therefore appears as secondary relatively to phylogenetic relationships in rhinos, which contradicts
495   our second hypothesis, postulating a stronger effect of mass over phylogeny on the patellar shape. Thus,
496   despite the central functional role of this bone in the knee, and the high stress linked to body mass exerted
497   on this joint, the influence of the weight is much more limited than expected.

498   Variation linked to size mainly affects the base, the medial angle, and the lateral edge of the patella, as
499   well as the cranial surface. All these areas are insertions for powerful knee extensors, respectively the *m.*
500   *rectus femoris*, the *m. vastus medialis*, the *m. vastus lateralis* (all three, together with the *m. vastus*
501   *intermedius*, forming the *m. quadriceps*) and the *m. gluteobiceps* (Etienne, Houssaye & Hutchinson,
502   2021) (Figure 1). The flattening of the base and the general craniocaudal broadening of the patella in
503   heavy rhino species likely provide more surface area for the insertion of stronger *m. rectus femoris* and *m.*
504   *gluteobiceps*, while in lighter rhinos the dorsal development of the base seems to increase the attachment
505   surface for the *m. vastus lateralis* and *m. vastus medialis* instead. This configuration may reflect that
506   heavy rhinos rely more on central hip muscles, such as the *m. rectus femoris,* to stabilize the knee while
507   lighter rhinos rely on medial and caudal muscles of the *m. quadriceps*, maybe ensuring more
508   manoeuvrability for this joint. Unfortunately, the scarcity of myological data for lighter rhino species
509   (Etienne, Houssaye & Hutchinson, 2021) and the lack of *in vivo* observations prevent us from making
510   further inference between the patellar shape and its relation to attached muscles.

511   The allometric relation is more strongly marked when considering all perissodactyls (Figure 10),
512   allometry accounting for 23% of the observed variation. However, body mass alone seems insufficient to
513   explain the shape variation among perissodactyls. A developed medial angle exists both in equids and
514   rhinos but not in tapirs, even though tapirs and equids are in the same range of body mass (hundreds of
515   kilograms), while rhinos can reach several tons (Table 1). Medial angle is associated with the presence of
516   a "knee locking" mechanism (Shockey, 2001; Schuurman, Kersten & Weijs, 2003; Janis et al., 2012).
517   Largely studied through the anatomy of the distal femora, this mechanism has poorly been considered on
518   the patellar side (Kappelman, 1988; Hermanson & MacFadden, 1996; Janis et al., 2012; Etienne et al.,
519   2020a). Our results do confirm the high correspondence between the presence of a developed medial
520   angle on the patella and that of a developed medial trochlear ridge on the femur (Hermanson &
521   MacFadden, 1996; Mallet et al., 2019). This developed medial angle shared between equids and rhinos
522   therefore appears as convergent in the two clades, although it does not seem perfectly homologous.
523   Indeed, while the medial angle in equids is extended by a parapatellar cartilage on which the medial
524   patellar ligament attaches (Hermanson & MacFadden, 1996, fig. 2), this cartilage seems absent in
525   rhinoceroses (or is little developed – C. Etienne, pers. com.), where the bony angle is more extended
526   medially than in equids. As shown in our results, the medial angle in rhinos is more extended and ossified
527   medially compared to equids. This could be directly related to their higher body mass, making cartilage
528   alone insufficient to support the weight of the body and ensure an efficient "knee locking". This would be
529   in line with our fourth hypothesis, assuming different shapes of patella to ensure an efficient "knee
530   locking" mechanism between equids and rhinos.

531   Similarly, the craniocaudal development of the base in equids offers a larger surface area for insertions of
532   knee extensors, these muscles being more powerful in equids than in rhinos compared to the respective
533   size of these animals (Etienne, Houssaye & Hutchinson, 2021). Myological data lack for tapirs but the
534   reduced surface of the base likely indicates reduced muscle insertions and, therefore, weaker knee
535   extensors in these animals. Such a craniocaudal development shifts the insertion of the extensor muscles
536   away from the axis of rotation of the knee, thus increasing the moment arm of the joint and the muscular
537   efficiency. This craniocaudal development of the patella in equids likely underlines the extreme cursorial
538   specialization of this clade, while the condition in rhinos appears more as a trade-off between the support
539   of their high body mass, their ability to reach a relatively high speed, and their evolutionary legacy.

540   The convergent emergence of the knee asymmetry in these clades remain poorly understood among
541   ungulates, various authors having supposed a link with either locomotor habit, feeding behaviour or body
542   mass (Kappelman, 1988; Hermanson & MacFadden, 1996; Shockey, 2001; Shockey et al., 2008;
543   Danaher, Shockey & Mihlbachler, 2009; Janis et al., 2012; Mihlbachler et al., 2014; Etienne et al.,
544   2020a). Locomotor habit shows a marked dichotomy between these clades. Rhinos and equids both
545   practice a transverse gallop while tapirs practice rotatory gallop, involving different limb loadings during
546   the gallop phases (Economou et al., 2020). Rotatory gallop involves a phase where both hindlimbs hit the
547   ground, while this never happen in transverse gallop, leading to higher mechanical stress exerted into a
548   single limb in the latter gait. While equids present an extreme cursorial specialization associated with
549   relatively low mass (Carrano, 1999), weight-bearing rhinos are still able to reach high speed despite
550   weighting several tons (Alexander & Pond, 1992; Etienne, Houssaye & Hutchinson, 2021). An
551   asymmetrical patella could be related to the emergence of a similar gallop in both equids and rhinos,
552   compared to tapirs. Differences in body mass may then explain the further divergences existing in patellar
553   shape between these two clades practicing transverse gallop. Further investigations including a large set

554 of fossil perissodactyls are needed to sharpen the understanding of this puzzling feature and the functional
555 advantages of this presence or absence in ungulates.

556 ## Conclusion

557 Our investigation of the shape of the patella among modern rhinoceroses and related extant perissodactyls
558 reveals a higher interspecific than intraspecific morphological variation. Contrary to our predictions, and
559 despite its central functional role in the knee joint and its implication in locomotion, the patella is affected
560 poorly by variation of body mass between and within species. Rather, the patellar shape follows clear
561 morphotypes existing in each species and even more marked at the scale of the family. This strong shape
562 conservatism may be directly related to its developmental origin, shared with the femur, another bone
563 whose shape has been proved to be highly linked to phylogenetic affinities before functional constraints
564 in perissodactyls. Despite a strong evolutionary legacy leading to a relative shape inertia, the shared
565 presence of a medial angle in rhinos and equids constitutes a clear case of morphological convergence
566 highlighting that functional constraints are also at work on the shape of this sesamoid bone. This
567 asymmetric conformation of the patella is related to a "knee locking" mechanism and maybe to the shared
568 emergence of transverse gallop in both clades. Within this convergence, rhinos present in addition shape
569 modifications that may be related to the support of a heavy mass. Further investigations of the shape of
570 the patella among a larger set of extinct Perissodactyla may be helpful for better understanding the
571 morphofunctional evolution of this sesamoid bone in mammals.

572

573 ## Acknowledgments

588 3D models are deposited on the 3D online repository MorphoSource at the following address according to
589 the internal policies on 3D data of each institution:
590 https://www.morphosource.org/projects/000366286?locale=en

591 **References**

592 Abdala V, Vera MC, Ponssa ML. 2017. On the Presence of the Patella in Frogs. *The Anatomical Record*

593   300:1747–1755. DOI: 10.1002/ar.23629.

594 Adams DC. 2014. A generalized K statistic for estimating phylogenetic signal from shape and other high-

595   dimensional multivariate data. *Systematic Biology* 63:685–697. DOI: 10.1093/sysbio/syu030.

596 Adams DC, Otárola-Castillo E. 2013. geomorph: an r package for the collection and analysis of geometric

597   morphometric shape data. *Methods in Ecology and Evolution* 4:393–399. DOI: 10.1111/2041-

598   210X.12035.

599 Adams DC, Rohlf FJ, Slice DE. 2004. Geometric morphometrics: Ten years of progress following the

600   'revolution.' *Italian Journal of Zoology* 71:5–16. DOI: 10.1080/11250000409356545.

601 Adler D, Murdoch D. 2020. rgl: 3d visualization device system (OpenGL).

602 Aglietti P, Menchetti PPM. 1995. Biomechanics of the Patellofemoral Joint. In: Scuderi GR ed. *The*

603   *Patella*. New York, NY: Springer, 25–48. DOI: 10.1007/978-1-4612-4188-1_3.

604 Alexander RM, Dimery NJ. 1985. The significance of sesamoids and retro-articular processes for the

605   mechanics of joints. *Journal of Zoology* 205:357–371. DOI: https://doi.org/10.1111/j.1469-

606   7998.1985.tb05622.x.

607 Alexander RM, Pond CM. 1992. Locomotion and bone strength of the white rhinoceros, *Ceratotherium*

608   *simum*. *Journal of Zoology* 227:63–69. DOI: 10.1111/j.1469-7998.1992.tb04344.x.

609 Allen VR, Kambic RE, Gatesy SM, Hutchinson JR. 2017. Gearing effects of the patella (knee extensor

610   muscle sesamoid) of the helmeted guineafowl during terrestrial locomotion. *Journal of Zoology*

611   303:178–187. DOI: https://doi.org/10.1111/jzo.12485.

612 Anderson JF, Hall-Martin A, Russell DA. 1985. Long-bone circumference and weight in mammals, birds

613   and dinosaurs. *Journal of Zoology* 207:53–61. DOI: 10.1111/j.1469-7998.1985.tb04915.x.

614 Antoine P-O, Reyes MC, Amano N, Bautista AP, Chang C-H, Claude J, De Vos J, Ingicco T. 2021. A new

615   rhinoceros clade from the Pleistocene of Asia sheds light on mammal dispersals to the

616   Philippines. *Zoological Journal of the Linnean Society* 194:416–430. DOI:

617   10.1093/zoolinnean/zlab009.

618 Artec 3D. 2018. Artec Studio Professional.

619 Bai B, Meng J, Wang Y-Q, Wang H-B, Holbrook L. 2017. Osteology of The Middle Eocene Ceratomorph

620   *Hyrachyus modestus* (Mammalia, Perissodactyla). *Bulletin of the American Museum of Natural*

621   *History*:1–70. DOI: 10.1206/0003-0090-413.1.1.

622   Bai B, Meng J, Zhang C, Gong Y-X, Wang Y-Q. 2020. The origin of Rhinocerotoidea and phylogeny of

623   Ceratomorpha (Mammalia, Perissodactyla). *Communications Biology* 3:1–16. DOI:

624   10.1038/s42003-020-01205-8.

625   Barone R. 2010a. *Anatomie comparée des mammifères domestiques. Tome 2 : Arthrologie et myologie*.

626   Paris: Vigot Frères.

627   Barone R. 2010b. *Anatomie comparée des mammifères domestiques. Tome 1 : Ostéologie*. Paris: Vigot

628   Frères.

629   Biewener AA, Patek SN. 2018. *Animal Locomotion*. New York: Oxford University Press.

630   Bizarro AH. 1921. On Sesamoid and Supernumerary Bones of the Limbs. *Journal of Anatomy* 55:256–

631   268.

632   Blomberg SP, Garland T, Ives AR, Crespi B. 2003. Testing for phylogenetic signal in comparative data:

633   behavioral traits are more labile. *Evolution* 57:717–745. DOI: 10.1554/0014-

634   3820(2003)057[0717:TFPSIC]2.0.CO;2.

635   Botton-Divet L. 2017. The Form-Function relationships in the process of secondary adaptation to an

636   aquatic life. PhD Thesis Thesis. Paris: Université Sorbonne Paris Cité.

637   Botton-Divet L, Cornette R, Fabre A-C, Herrel A, Houssaye A. 2016. Morphological Analysis of Long Bones

638   in Semi-aquatic Mustelids and their Terrestrial Relatives. *Integrative and Comparative Biology*

639   56:1298–1309. DOI: 10.1093/icb/icw124.

640   Botton-Divet L, Cornette R, Houssaye A, Fabre A-C, Herrel A. 2017. Swimming and running: a study of

641   the convergence in long bone morphology among semi-aquatic mustelids (Carnivora:

642   Mustelidae). *Biological Journal of the Linnean Society* 121:38–49. DOI:

643   10.1093/biolinnean/blw027.

644   Campione NE. 2017. Extrapolating body masses in large terrestrial vertebrates. *Paleobiology* 43:693–

645   699. DOI: 10.1017/pab.2017.9.

646   Campione NE, Evans DC. 2012. A universal scaling relationship between body mass and proximal limb

647   bone dimensions in quadrupedal terrestrial tetrapods. *BMC Biology* 10:1–21. DOI:

648   10.1186/1741-7007-10-60.

649   Carrano MT. 1999. What, if anything, is a cursor? Categories versus continua for determining locomotor

650   habit in mammals and dinosaurs. *Journal of Zoology* 247:29–42. DOI: 10.1111/j.1469-

651   7998.1999.tb00190.x.

652   Chadwick KP, Regnault S, Allen V, Hutchinson JR. 2014. Three-dimensional anatomy of the ostrich

653   (*Struthio camelus*) knee joint. *PeerJ* 2:e706. DOI: 10.7717/peerj.706.

654   Cignoni P, Callieri M, Corsini M, Dellepiane M, Ganovelli F, Ranzuglia G. 2008. *MeshLab: an Open-Source*

655   *Mesh Processing Tool*. The Eurographics Association. DOI:

656   http://dx.doi.org/10.2312/LocalChapterEvents/ItalChap/ItalianChapConf2008/129-136.

657   Cirilli O, Pandolfi L, Rook L, Bernor RL. 2021. Evolution of Old World *Equus* and origin of the zebra-ass

658   clade. *Scientific Reports* 11:10156. DOI: 10.1038/s41598-021-89440-9.

659   Corina Vera M, Laura Ponssa M, Abdala V. 2015. Further Data on Sesamoid Identity from Two Anuran

660   Species. *The Anatomical Record* 298:1376–1394. DOI: 10.1002/ar.23158.

661   Damuth JD, MacFadden BJ. 1990. *Body Size in Mammalian Paleobiology: Estimation and Biological*

662   *Implications*. Cambridge University Press.

663   Dan M, Parr W, Broe D, Cross M, Walsh WR. 2018. Biomechanics of the knee extensor mechanism and

664   its relationship to patella tendinopathy: A review. *Journal of Orthopaedic Research* 36:3105–

665   3112. DOI: https://doi.org/10.1002/jor.24120.

666   Danaher K, Shockey BJ, Mihlbachler MC. 2009. Perissodactyl patella: morphological variation and

667   phylogenetic signifiance in a neglected element. *Journal of Vertebrate Paleontology* 29:85A.

668   Dinerstein E. 1991. Sexual Dimorphism in the Greater One-Horned Rhinoceros (*Rhinoceros unicornis*).

669   *Journal of Mammalogy* 72:450–457. DOI: 10.2307/1382127.

670   Dinerstein E. 2011. Family Rhinocerotidae (Rhinoceroses). In: Wilson DE, Mittermeier RA eds. *Handbook*

671   *of the Mammals of the World*. Barcelona: Don E. Wilson & Russel A. Mittermeier, 144–181.

672   Economou G, McGrath M, Wajsberg J, Granatosky MC. 2020. Perissodactyla Locomotion. In: Vonk J,

673   Shackelford T eds. *Encyclopedia of Animal Cognition and Behavior*. Cham: Springer International

674   Publishing, 1–8. DOI: 10.1007/978-3-319-47829-6_887-1.

675   Eisenmann V, Guérin C. 1984. Morphologie fonctionnelle et environnement chez les périssodactyles.

676   *Geobios* 17:69–74. DOI: 10.1016/S0016-6995(84)80158-8.

677   Ellis MI, Seedhom BB, Wright V, Dowson D. 1980. An Evaluation of the Ratio between the Tensions along

678   the Quadriceps Tendon and the Patellar Ligament. *Engineering in Medicine* 9:189–194. DOI:

679   10.1243/EMED_JOUR_1980_009_049_02.

680   Etienne C, Filippo A, Cornette R, Houssaye A. 2020a. Effect of mass and habitat on the shape of limb long

681   bones: A morpho-functional investigation on Bovidae (Mammalia: Cetartiodactyla). *Journal of*

682   *Anatomy* 238:886–904. DOI: https://doi.org/10.1111/joa.13359.

683   Etienne C, Houssaye A, Hutchinson JR. 2021. Limb myology and muscle architecture of the Indian

684   rhinoceros *Rhinoceros unicornis* and the white rhinoceros *Ceratotherium simum* (Mammalia:

685   Rhinocerotidae). *PeerJ* 9:e11314. DOI: 10.7717/peerj.11314.

686 Etienne C, Mallet C, Cornette R, Houssaye A. 2020b. Influence of mass on tarsus shape variation: a

687   morphometrical investigation among Rhinocerotidae (Mammalia: Perissodactyla). *Biological*

688   *Journal of the Linnean Society* 129:950–974. DOI: 10.1093/biolinnean/blaa005.

689 Eyal S, Blitz E, Shwartz Y, Akiyama H, Schweitzer R, Zelzer E. 2015. On the development of the patella.

690   *Development* 142:1831–1839. DOI: 10.1242/dev.121970.

691 Eyal S, Rubin S, Krief S, Levin L, Zelzer E. 2019. Common cellular origin and diverging developmental

692   programs for different sesamoid bones. *Development* 146:dev167452. DOI:

693   10.1242/dev.167452.

694 Fabre A-C, Cornette R, Peigné S, Goswami A. 2013. Influence of body mass on the shape of forelimb in

695   musteloid carnivorans. *Biological Journal of the Linnean Society* 110:91–103. DOI:

696   10.1111/bij.12103.

697 Federative Committee on Anatomical Terminology. 1998. *Terminologia Anatomica*. Georg Thieme

698   Verlag.

699 Garnoeva R. 2022. Patellar Morphology in Small Breed Dogs With Medial Patellar Luxation. *Egyptian*

700   *Journal of Veterinary Sciences* 53:403–408. DOI: 10.21608/ejvs.2022.121266.1327.

701 Goodall C. 1991. Procrustes Methods in the Statistical Analysis of Shape. *Journal of the Royal Statistical*

702   *Society: Series B (Methodological)* 53:285–321. DOI: 10.1111/j.2517-6161.1991.tb01825.x.

703 Gould SJ. 2002. *The Structure of Evolutionary Theory*. Cambridge, Massachusetts; London, England:

704   Harvard University Press.

705 Gower JC. 1975. Generalized procrustes analysis. *Psychometrika* 40:33–51. DOI: 10.1007/BF02291478.

706 Guérin C. 1980. Les Rhinocéros (Mammalia, Perissodactyla) du Miocène terminal au Pléistocène

707   supérieur en Europe occidentale. Comparaison avec les espèces actuelles. Documents du

708   Laboratoire de Géologie de l'Université de Lyon Thesis.

709 Gunz P, Mitteroecker P. 2013. Semilandmarks: a method for quantifying curves and surfaces. *Hystrix, the*

710   *Italian Journal of Mammalogy* 24:103–109.

711 Gunz P, Mitteroecker P, Bookstein FL. 2005. Semilandmarks in Three Dimensions. In: Slice DE ed.

712   *Modern Morphometrics in Physical Anthropology*. Developments in Primatology: Progress and

713   Prospects. Boston, MA: Slice, D. E., 73–98. DOI: 10.1007/0-387-27614-9_3.

714 Hallgrímsson B, Jamniczky H, Young NM, Rolian C, Parsons TE, Boughner JC, Marcucio RS. 2009.

715   Deciphering the Palimpsest: Studying the Relationship Between Morphological Integration and

716   Phenotypic Covariation. *Evolutionary Biology* 36:355–376. DOI: 10.1007/s11692-009-9076-5.

717   Hanot P, Herrel A, Guintard C, Cornette R. 2017. Morphological integration in the appendicular skeleton

718   of two domestic taxa: the horse and donkey. *Proc. R. Soc. B* 284:20171241. DOI:

719   10.1098/rspb.2017.1241.

720   Hanot P, Herrel A, Guintard C, Cornette R. 2018. The impact of artificial selection on morphological

721   integration in the appendicular skeleton of domestic horses. *Journal of Anatomy* 232:657–673.

722   DOI: 10.1111/joa.12772.

723   Hermanson JW, MacFadden BJ. 1996. Evolutionary and functional morphology of the knee in fossil and

724   extant horses (Equidae). *Journal of Vertebrate Paleontology* 16:349–357. DOI:

725   10.1080/02724634.1996.10011321.

726   Hildebrand M. 1974. *Analysis of vertebrate structure*. New York: John Wiley & Sons.

727   Ho J, Tumkaya T, Aryal S, Choi H, Claridge-Chang A. 2019. Moving beyond P values: data analysis with

728   estimation graphics. *Nature Methods* 16:565–566. DOI: 10.1038/s41592-019-0470-3.

729   Houssaye A, Perthuis A de, Houée G. 2021. Sesamoid bones also show functional adaptation in their

730   microanatomy—The example of the patella in Perissodactyla. *Journal of Anatomy* n/a. DOI:

731   10.1111/joa.13530.

732   Janis CM, Shoshitaishvili B, Kambic R, Figueirido B. 2012. On their knees: distal femur asymmetry in

733   ungulates and its relationship to body size and locomotion. *Journal of Vertebrate Paleontology*

734   32:433–445. DOI: 10.1080/02724634.2012.635737.

735   Jerez A, Mangione S, Abdala V. 2010. Occurrence and distribution of sesamoid bones in squamates: a

736   comparative approach. *Acta Zoologica* 91:295–305. DOI: 10.1111/j.1463-6395.2009.00408.x.

737   Kappelman J. 1988. Morphology and locomotor adaptations of the bovid femur in relation to habitat.

738   *Journal of Morphology* 198:119–130. DOI: 10.1002/jmor.1051980111.

739   Klingenberg CP. 2016. Size, shape, and form: concepts of allometry in geometric morphometrics.

740   *Development Genes and Evolution* 226:113–137. DOI: 10.1007/s00427-016-0539-2.

741   Liu S, Westbury MV, Dussex N, Mitchell KJ, Sinding M-HS, Heintzman PD, Duchêne DA, Kapp JD, Seth J

742   von, Heiniger H, Sánchez-Barreiro F, Margaryan A, André-Olsen R, Cahsan BD, Meng G, Yang C,

743   Chen L, Valk T van der, Moodley Y, Rookmaaker K, Bruford MW, Ryder O, Steiner C, Sonsbeek

744   LGRB, Vartanyan S, Guo C, Cooper A, Kosintsev P, Kirillova I, Lister AM, Marques-Bonet T,

745   Gopalakrishnan S, Dunn RR, Lorenzen ED, Shapiro B, Zhang G, Antoine P-O, Dalén L, Gilbert MTP.

746   2021. Ancient and modern genomes unravel the evolutionary history of the rhinoceros family.

747   *Cell* 184:4874-4885.e16. DOI: 10.1016/j.cell.2021.07.032.

748 Lovejoy CO. 2007. The natural history of human gait and posture: Part 3. The knee. *Gait & Posture*
749   25:325–341. DOI: 10.1016/j.gaitpost.2006.05.001.

750 MacLaren JA, Hulbert Jr RC, Wallace SC, Nauwelaerts S. 2018. A morphometric analysis of the forelimb in
751   the genus *Tapirus* (Perissodactyla: Tapiridae) reveals influences of habitat, phylogeny and size
752   through time and across geographical space. *Zoological Journal of the Linnean Society* 20:1–17.

753 MacLaren JA, Nauwelaerts S. 2016. A three-dimensional morphometric analysis of upper forelimb
754   morphology in the enigmatic tapir (Perissodactyla: *Tapirus*) hints at subtle variations in
755   locomotor ecology. *Journal of Morphology* 277:1469–1485. DOI: 10.1002/jmor.20588.

756 MacLaren JA, Nauwelaerts S. 2017. Interspecific variation in the tetradactyl manus of modern tapirs
757   (Perissodactyla: *Tapirus*) exposed using geometric morphometrics. *Journal of Morphology*
758   278:1517–1535. DOI: 10.1002/jmor.20728.

759 Mallet C, Billet G, Cornette R, Alexandra Houssaye A. 2022. Adaptation to graviportality in
760   Rhinocerotoidea? An investigation through the long bone shape variation in their hindlimb.
761   *Zoological Journal of the Linnean Society* 196:1235–1271. DOI: 10.1093/zoolinnean/zlac007.

762 Mallet C, Billet G, Houssaye A, Cornette R. 2020. A first glimpse at the influence of body mass in the
763   morphological integration of the limb long bones: an investigation in modern rhinoceroses.
764   *Journal of Anatomy* 237:704–726. DOI: 10.1111/joa.13232.

765 Mallet C, Cornette R, Billet G, Houssaye A. 2019. Interspecific variation in the limb long bones among
766   modern rhinoceroses—extent and drivers. *PeerJ* 7:e7647. DOI: 10.7717/peerj.7647.

767 Mallet C, Houssaye A, Cornette R, Billet G. 2021. Long bone shape variation in the forelimb of
768   Rhinocerotoidea – Relation with size, body mass and body proportions. *Zoological Journal of the*
769   *Linnean Society* 196:1201–1234. DOI: 10.1093/zoolinnean/zlab095.

770 Medici EP. 2011. Family Tapiridae (Tapirs). In: Wilson DE, Mittermeier RA eds. *Handbook of the*
771   *mammals of the world*. Barcelona: Lynx Edicions, 182–203.

772 Mihlbachler MC, Lau T, Kapner D, Shockey BJ. 2014. Coevolution of the shoulder and knee in Ungulates:
773   Implications of the evolution of locomotion and standing.

774 Mitteroecker P, Gunz P, Windhager S, Schaefer K. 2013. A brief review of shape, form, and allometry in
775   geometric morphometrics, with applications to human facial morphology. *Hystrix, the Italian*
776   *Journal of Mammalogy* 24:59–66. DOI: 10.4404/hystrix-24.1-6369.

777 Mitteroecker P, Schaefer K. 2022. Thirty years of geometric morphometrics: Achievements, challenges,
778   and the ongoing quest for biological meaningfulness. *American Journal of Biological*
779   *Anthropology* 178:181–210. DOI: 10.1002/ajpa.24531.

780 Pandolfi L, Antoine P-O, Bukhsianidze M, Lordkipanidze D, Rook L. 2021. Northern Eurasian
781   rhinocerotines (Mammalia, Perissodactyla) by the Pliocene–Pleistocene transition: phylogeny
782   and historical biogeography. *Journal of Systematic Palaeontology*:1–27. DOI:
783   10.1080/14772019.2021.1995907.

784 Pina M, DeMiguel D, Puigvert F, Marcé-Nogué J, Moyà-Solà S. 2020. Knee function through finite
785   element analysis and the role of Miocene hominoids in our understanding of the origin of
786   antipronograde behaviours: the *Pierolapithecus catalaunicus* patella as a case study.
787   *Palaeontology* 63:459–475. DOI: https://doi.org/10.1111/pala.12466.

788 Pintore R, Houssaye A, Nesbitt SJ, Hutchinson JR. 2021. Femoral specializations to locomotor habits in
789   early archosauriforms. *Journal of Anatomy* 240:867–892. DOI: 10.1111/joa.13598.

790 Polly PD. 2007. Limbs in mammalian evolution. Chapter 15. In: Hall BK ed. *Fins into Limbs: Evolution,*
791   *Development, and Transformation*. Chicago: Brian K. Hall, 245–268.

792 Ponssa ML, Goldberg J, Abdala V. 2010. Sesamoids in Anurans: New Data, Old Issues. *The Anatomical*
793   *Record* 293:1646–1668. DOI: 10.1002/ar.21212.

794 R Core Team. 2014. R: a language and environment for statistical computing.

795 Raux P, Townsend PR, Miegel R, Rose RM, Radin EL. 1975. Trabecular architecture of the human patella.
796   *Journal of Biomechanics* 8:1–7. DOI: 10.1016/0021-9290(75)90037-8.

797 Raymond KR, Prothero DR. 2012. Comparative variability of intermembranous and endochondral bones
798   in Pleistocene mammals. *Palaeontologia Electronica* 13:14.

799 Revell LJ. 2012. phytools: an R package for phylogenetic comparative biology (and other things).
800   *Methods in Ecology and Evolution* 3:217–223. DOI: 10.1111/j.2041-210X.2011.00169.x.

801 Rohlf FJ, Slice D. 1990. Extensions of the Procrustes Method for the Optimal Superimposition of
802   Landmarks. *Systematic Biology* 39:40–59. DOI: 10.2307/2992207.

803 Rubenstein DI. 2011. Family Equidae (Horses and relatives). In: Wilson DE, Mittermeier RA eds.
804   *Handbook of the mammals of the world*. Barcelona: Lynx Edicions, 106–143.

805 Samuels ME, Regnault S, Hutchinson JR. 2017. Evolution of the patellar sesamoid bone in mammals.
806   *PeerJ* 5:e3103. DOI: 10.7717/peerj.3103.

807 Schlager S. 2017. Chapter 9 - Morpho and Rvcg – Shape Analysis in R: R-Packages for Geometric
808   Morphometrics, Shape Analysis and Surface Manipulations. In: Zheng G, Li S, Székely G eds.
809   *Statistical Shape and Deformation Analysis*. Academic Press, 217–256. DOI: 10.1016/B978-0-12-
810   810493-4.00011-0.

811   Schneider MT-Y, Rooks N, Besier T. 2022. Cartilage thickness and bone shape variations as a function of

812   sex, height, body mass, and age in young adult knees. *Scientific Reports* 12:11707. DOI:

813   10.1038/s41598-022-15585-w.

814   Schuurman SO, Kersten W, Weijs WA. 2003. The equine hind limb is actively stabilized during standing.

815   *Journal of Anatomy* 202:355–362. DOI: 10.1046/j.1469-7580.2003.00166.x.

816   Scott KM. 1990. Postcranial dimensions of ungulates as predictors of body mass. In: Damuth JD,

817   MacFadden BJ eds. *Body Size in Mammalian Palaeobiology: Estimation and Biological*

818   *Implications*. Cambridge University Press, 301–335.

819   Seilacher A. 1970. Arbeitskonzept Zur Konstruktions-Morphologie. *Lethaia* 3:393–396. DOI:

820   10.1111/j.1502-3931.1970.tb00830.x.

821   Seilacher A. 1991. Self-Organizing Mechanisms in Morphogenesis and Evolution. In: Schmidt-Kittler N,

822   Vogel K eds. *Constructional Morphology and Evolution*. Berlin, Heidelberg: Springer, 251–271.

823   DOI: 10.1007/978-3-642-76156-0_17.

824   Serio C, Raia P, Meloro C. 2020. Locomotory Adaptations in 3D Humerus Geometry of Xenarthra: Testing

825   for Convergence. *Frontiers in Ecology and Evolution* 8. DOI: 10.3389/fevo.2020.00139.

826   Shockey BJ. 2001. Specialized knee joints in some extinct, endemic, South American herbivores. *Acta*

827   *Palaeontologica Polonica* 46:277–288.

828   Shockey BJ, Mihlbachler MC, Solounias N, Hayes BP. 2008. Functional morphology of the knee in rhinos

829   and the evolution of knee locking mechanisms among rhinocerotoid perissodactyls. *Journal of*

830   *Vertebrate Paleontology* 28:142A.

831   Steiner CC, Ryder OA. 2011. Molecular phylogeny and evolution of the Perissodactyla. *Zoological Journal*

832   *of the Linnean Society* 163:1289–1303. DOI: 10.1111/j.1096-3642.2011.00752.x.

833   Tallman M. 2016. Shape Ontogeny of the Distal Femur in the Hominidae with Implications for the

834   Evolution of Bipedality. *PLOS ONE* 11:e0148371. DOI: 10.1371/journal.pone.0148371.

835   Thermo Fisher Scientific. 2018. Avizo.

836   Toumi H, Higashiyama I, Suzuki D, Kumai T, Bydder G, McGonagle D, Emery P, Fairclough J, Benjamin M.

837   2006. Regional variations in human patellar trabecular architecture and the structure of the

838   proximal patellar tendon enthesis. *Journal of Anatomy* 208:47–57. DOI:

839   https://doi.org/10.1111/j.1469-7580.2006.00501.x.

840   Valois H. 1917. La valeur morphologique de la rotule chez les mammifères. *Bulletins et Mémoires de la*

841   *Société d'Anthropologie de Paris* 8:1–34. DOI: 10.3406/bmsap.1917.8819.

842   Vickaryous MK, Olson WM. 2008. Sesamoids and ossicles in the appendicular skeleton. In: Hall BK ed.

843   *Fins into Limbs: Evolution, Development, and Transformation*. Chicago: University of Chicago

844   Press, 323–341.

845   Wasserstein RL, Schirm AL, Lazar NA. 2019. Moving to a World Beyond "p < 0.05." *The American*

846   *Statistician* 73:1–19. DOI: 10.1080/00031305.2019.1583913.

847   Wiley DF, Amenta N, Alcantara DA, Ghosh D, Kil YJ, Delson E, Harcourt-Smith W, Rohlf FJ, St. John K,

848   Hamann B. 2005. Evolutionary Morphing. In: *Proceedings of IEEE Visualization 2005*.

849   Minneapolis, Minnesota,.

850   Zelditch ML, Swiderski DL, Sheets HD, Fink WL. 2012. *Geometric morphometrics for biologists: A Primer*.

851   Academic Press.

852   Zschokke S, Baur B. 2002. Inbreeding, outbreeding, infant growth, and size dimorphism in captive Indian

853   rhinoceros (*Rhinoceros unicornis*). *Canadian Journal of Zoology* 80:2014–2023. DOI:

854   10.1139/z02-183.

855

Figure 1

Main muscular insertions on the patella of a white rhinoceros (*Ceratotherium simum*).

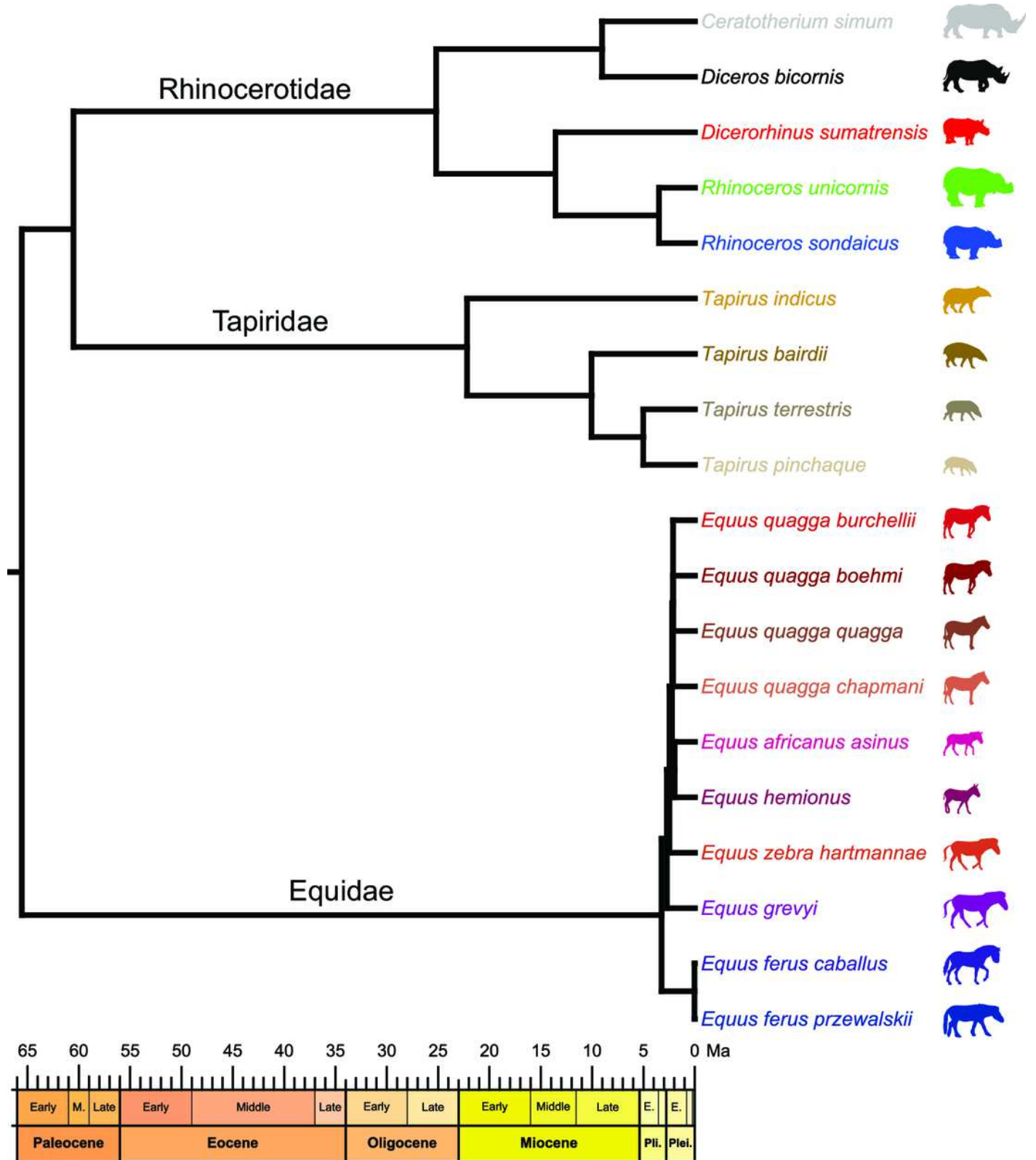Derived from Barone 2010a and Etienne et al., 2021.
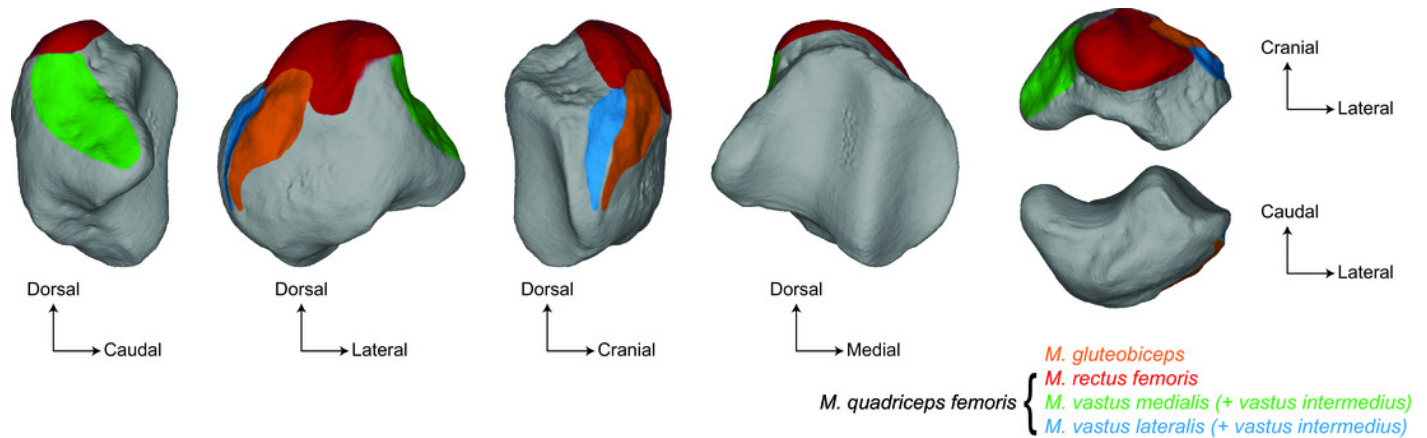
Figure 2

Composite cladogram of the sampled species.

Branch lengths and relations based on Steiner & Ryder, 2011; MacLaren et al., 2018; Bai et al., 2020; Cirilli et al., 2021; Antoine et al., 2021; Liu et al., 2021; Pandolfi et al., 2021 . Silhouettes provided by *www.phylopic.org* under the Creative Commons license.
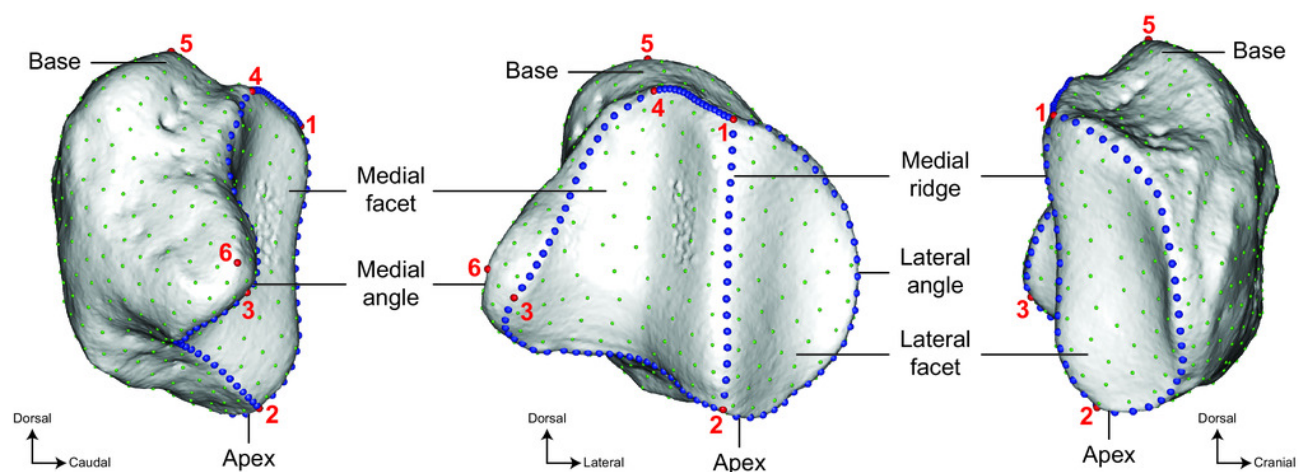
Figure 3

Location of the landmarks used for the analyses.

6 anatomical landmarks (red spheres), 103 curve sliding (blue spheres) and 461 surface sliding (green spheres) semi-landmarks were placed on the patella. Designation of the anatomical landmarks – 1: Most proximal point of the medial ridge; 2: Most distal point of the medial ridge; 3: Most medial point of the medial articular surface; 4: Most proximal point of the medial articular surface; 5: Most proximal point of the base; 6: Most medial point of the medial angle.

Figure 4

Neighbour Joining tree computed on all PC scores obtained from the PCA performed on shape data of adult rhinoceroses
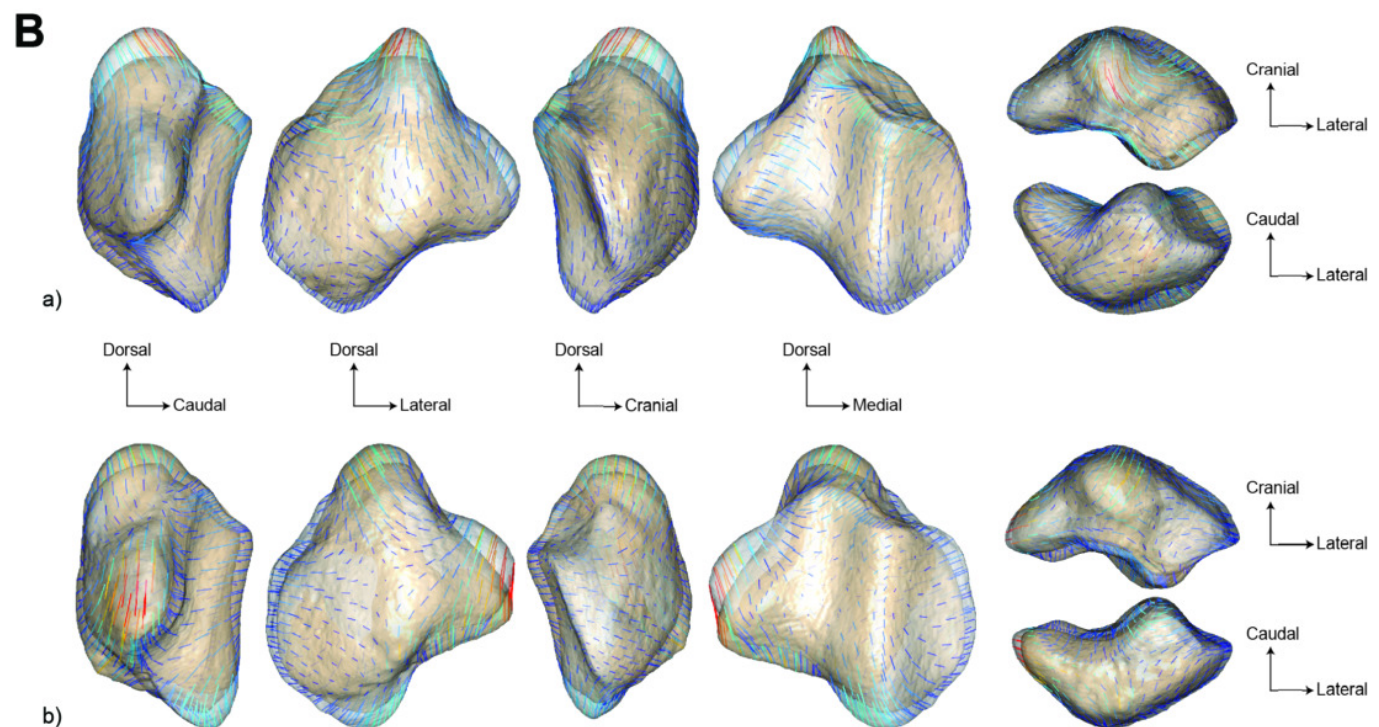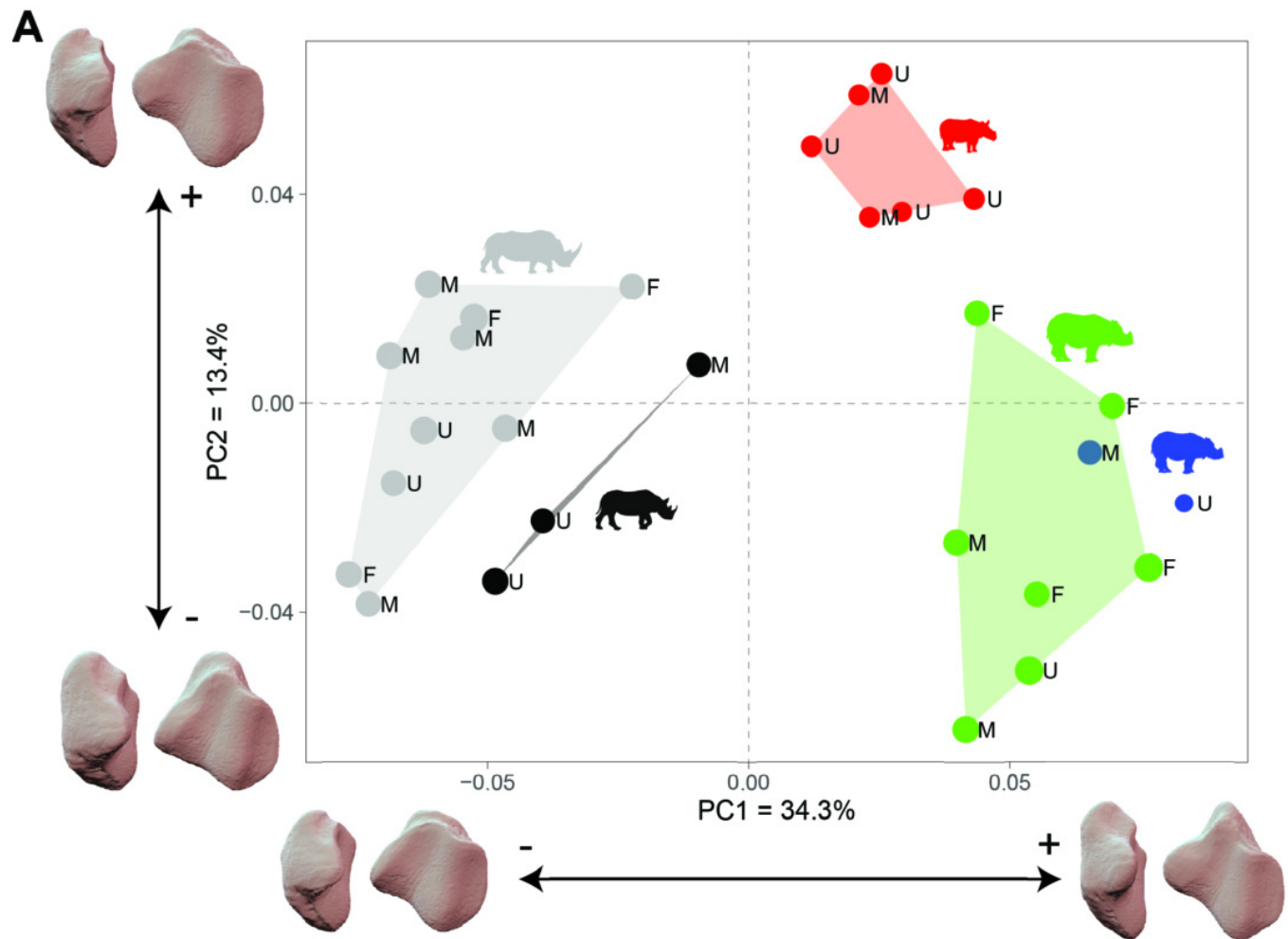
Colour code follows Figure 2. Letters indicate sex attribution as in Table 1 (F: female; M: male; U: unknown). Point size is proportional to the mean log centroid size of each specimen.
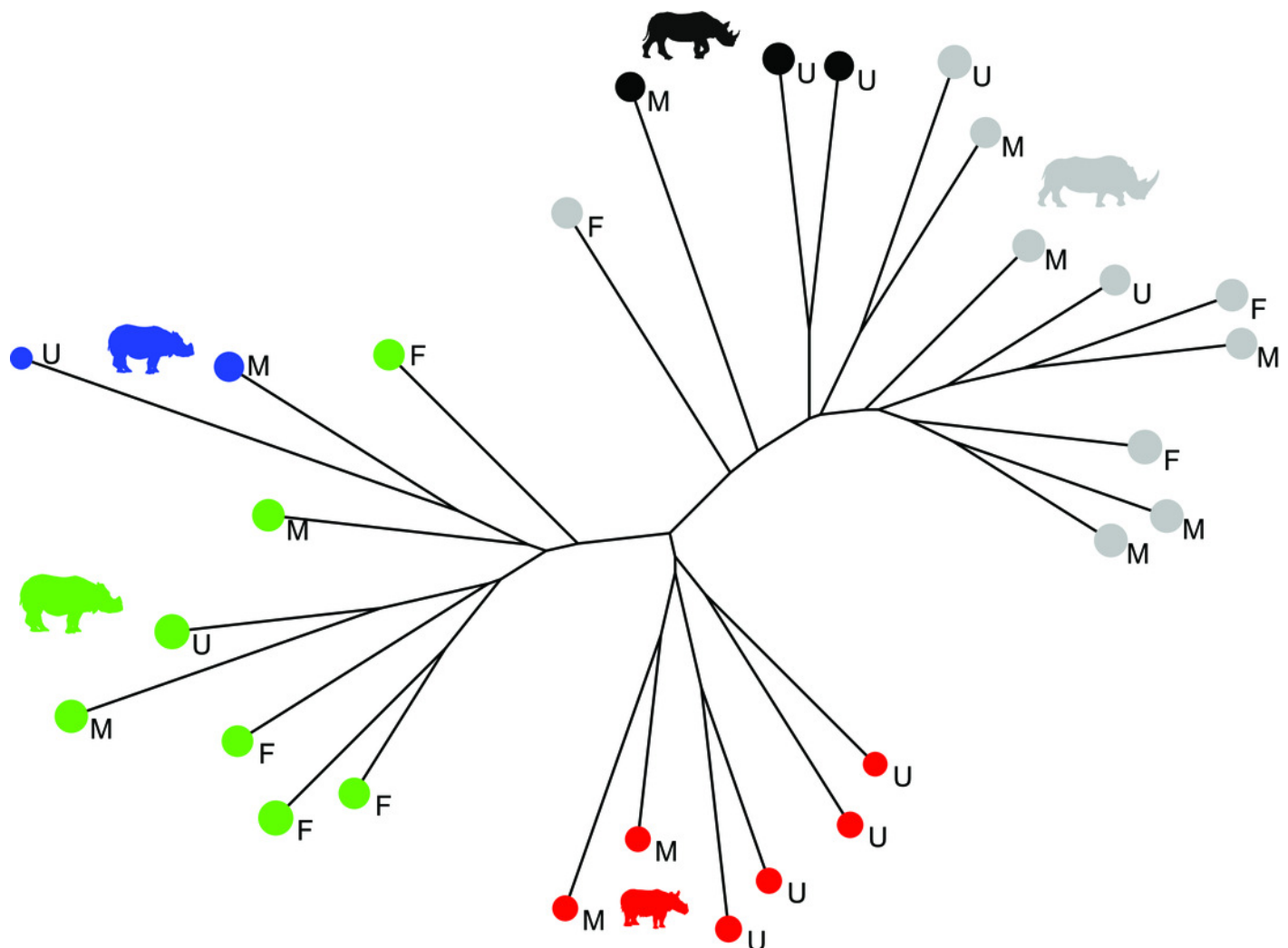
Figure 5

Results of the PCA performed on morphometric data of adult rhinoceroses and associated shape variation.
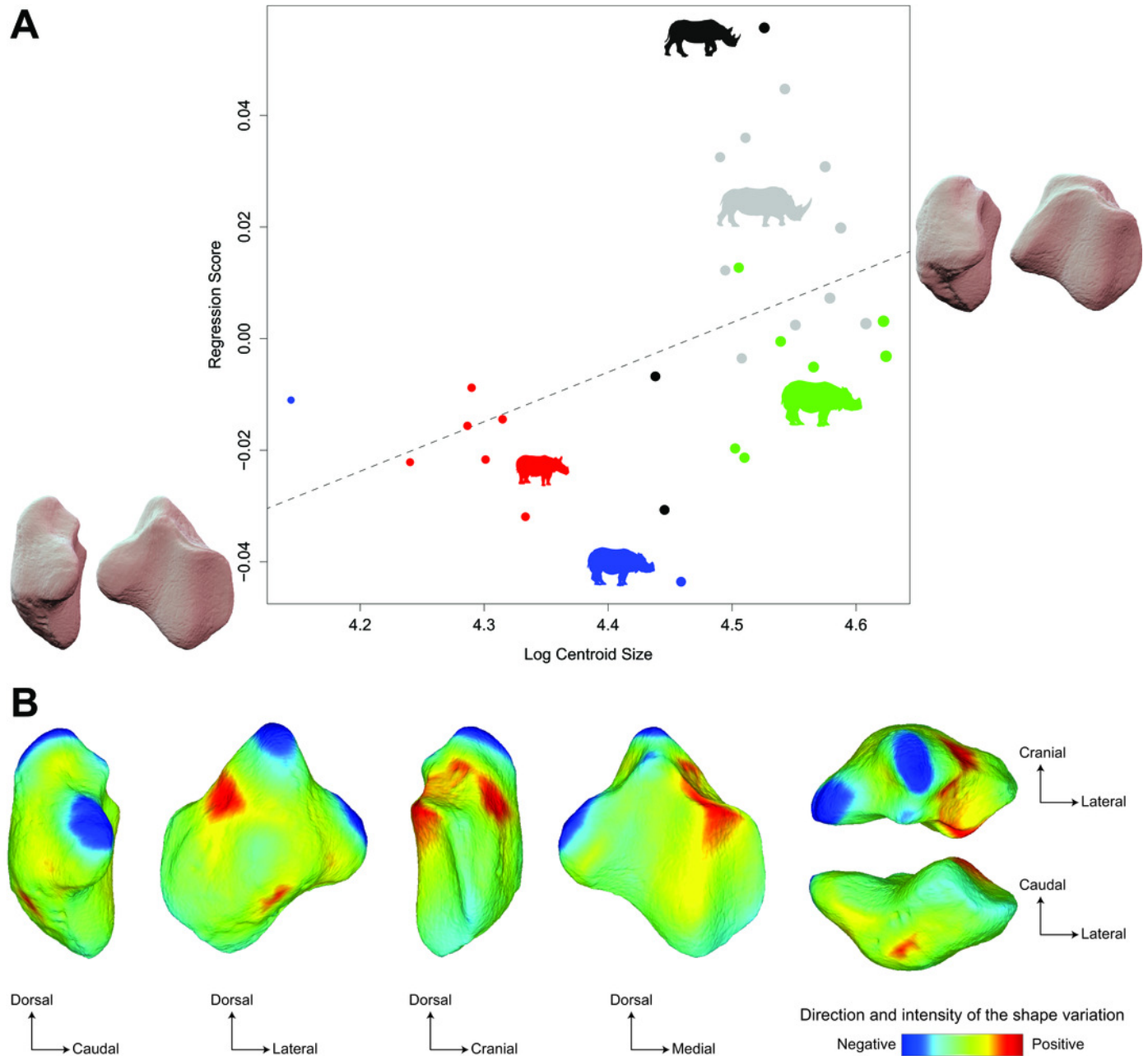
A: Biplot of the two first axes of the PCA with minimal and maximal theoretical shape associated with this variation (respectively in medial and caudal views). Colour codes follow Figure 2. Letters indicate sex attribution as in Table 1. Point size is proportional to the mean log centroid size of each specimen. **B**: Morphological variation between minimal (light brown) and maximal (light grey) theoretical shapes along a) PC1 and b) PC2 respectively in medial, cranial, lateral, caudal, dorsal (top) and ventral (bottom) views. Intensities of landmark displacements are shown with vector colorations ranging from blue (low distance) to red (high distance).

Figure 6

Results of the Procrustes ANOVA on shape data against log-transformed centroid size (CS) for adult rhinos.

A: Regression plot with theoretical shapes associated with minimum and maximum fitted values (respectively in medial and caudal views). Colour code follows Figure 2. Point size is proportional to the mean log centroid size of each specimen. **B:** Colour maps of the location and intensity of the shape deformation. The shape associated with the maximal CS value of the Procrustes ANOVA was coloured depending on its distance to the shape associated with the minimal value. Green indicates no deformation; blue indicates a negative deformation of high intensity; red indicates a positive deformation of high intensity.

A

B

Dorsal → Caudal

Dorsal → Lateral

Dorsal → Cranial

Dorsal → Medial

Cranial → Lateral

Caudal → Lateral

Direction and intensity of the shape variation

Negative ▮▮▮ Positive

Figure 7

Shape variation among all rhinoceroses (adults and subadults).

A: Neighbour Joining tree computed on all PC scores obtained from the PCA performed on shape data. Colour code follows Figure 2. Symbols indicate age class as in Table 1 (triangle: subadult; circle: adult). Point size is proportional to the mean log centroid size of each specimen. **B**: Biplot of the two first axes of the PCA with minimal and maximal theoretical shape associated with this variation (respectively in medial and caudal views). Colour codes follow Figure 2. Letters indicate sex attribution as in Table 1 (F: female; M: male; U: unknown). Point size is proportional to the mean log centroid size of each specimen.
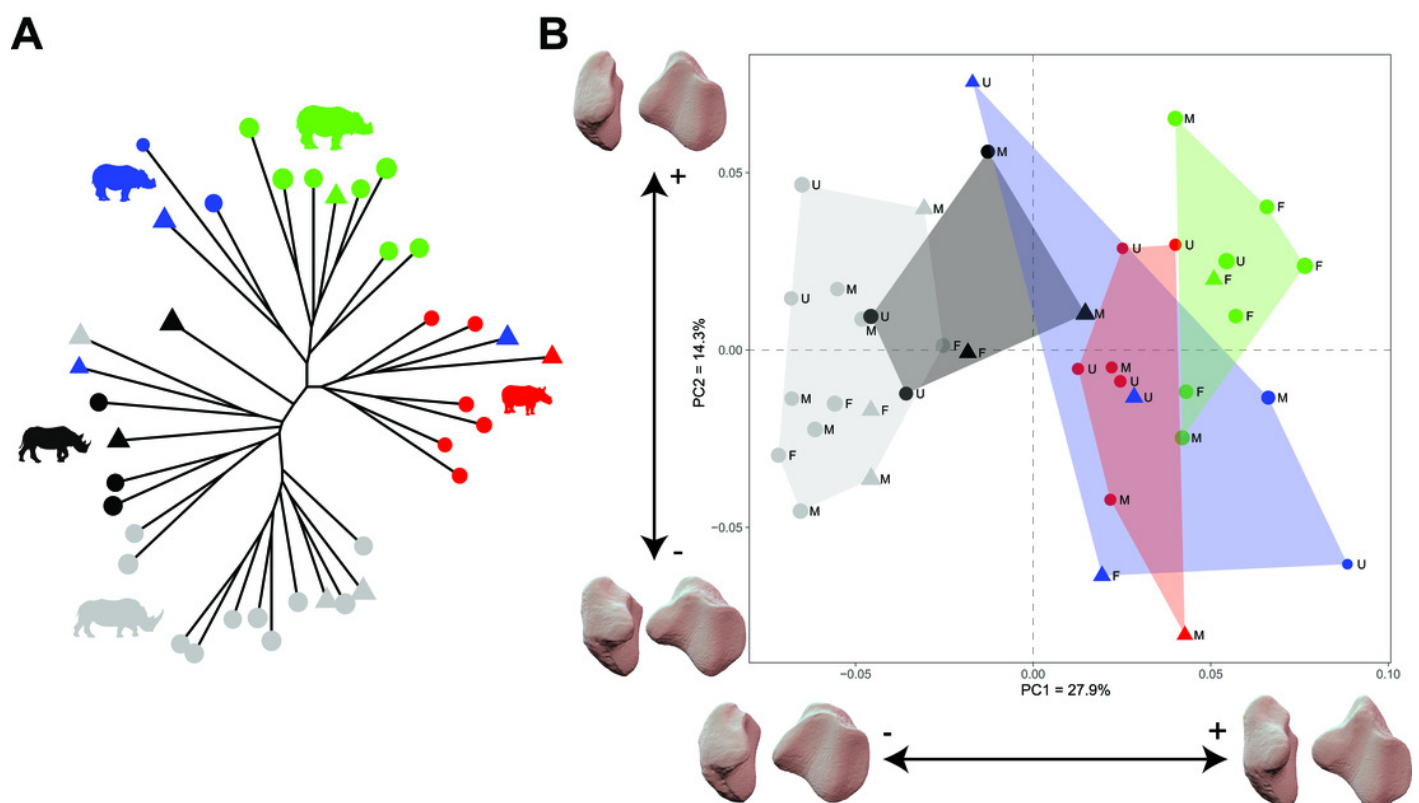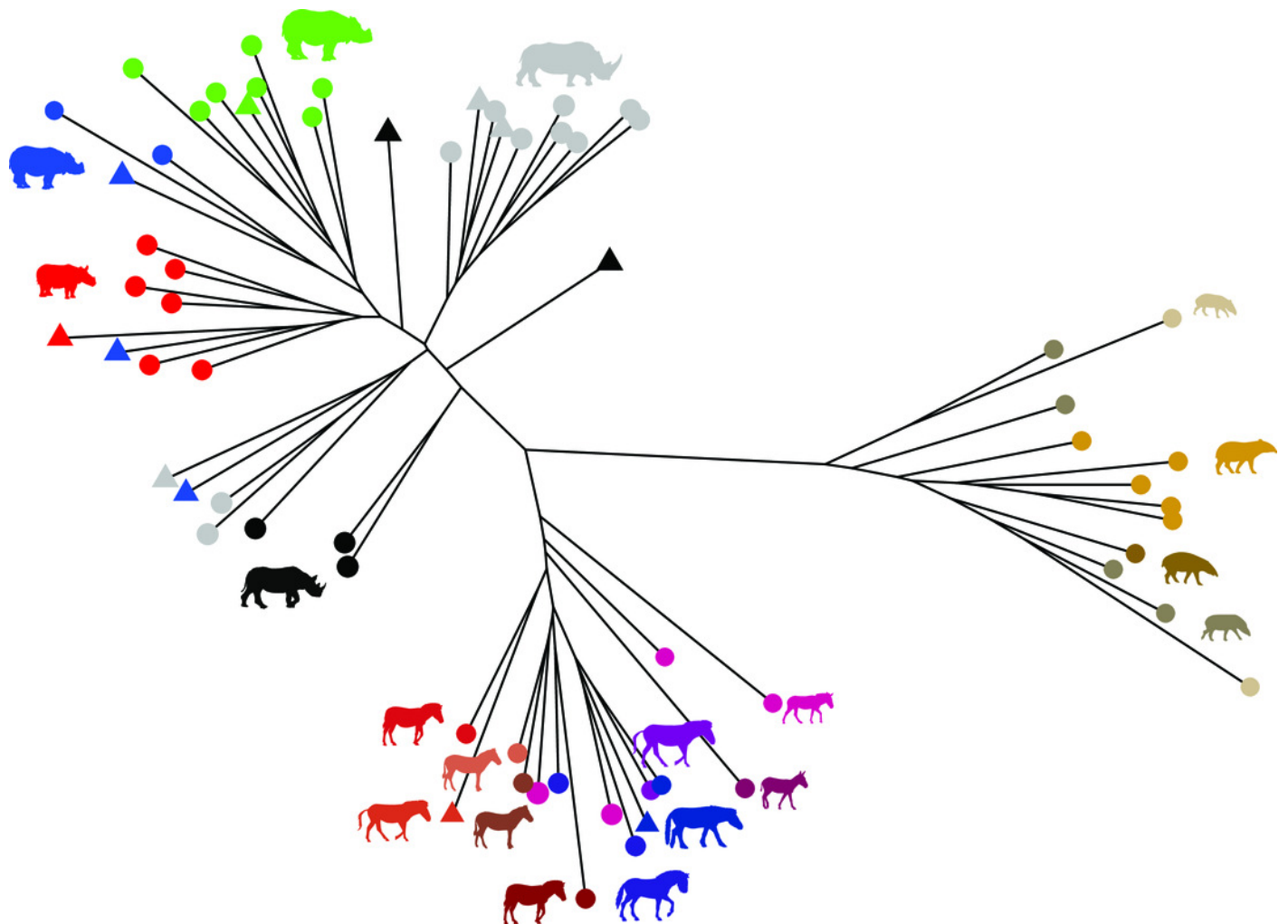
Figure 8

Neighbour Joining tree computed on all PC scores obtained from the PCA performed on shape data of all perissodactyls.

Colour code follows Figure 2. Symbols indicate age class as in Table 1 (triangle: subadult; circle: adult). Point size is proportional to the mean log centroid size of each specimen.

Figure 9

Results of the PCA performed on morphometric data of all perissodactyls and associated shape variation.

A: Biplot of the two first axes of the PCA with minimal and maximal theoretical shape associated with this variation (respectively in medial and caudal views). Colour codes follow Figure 2. Symbols indicate age class as in Table 1 (triangle: subadult; circle: adult). Point size is proportional to the mean log centroid size of each specimen. **B**: Morphological variation between minimal (light brown) and maximal (light grey) theoretical shapes along a) PC1 and b) PC2 respectively in medial, cranial, lateral, caudal, dorsal (top) and ventral (bottom) views. Intensities of landmark displacements are shown with vector colorations ranging from blue (low distance) to red (high distance).

A

B

a)

b)
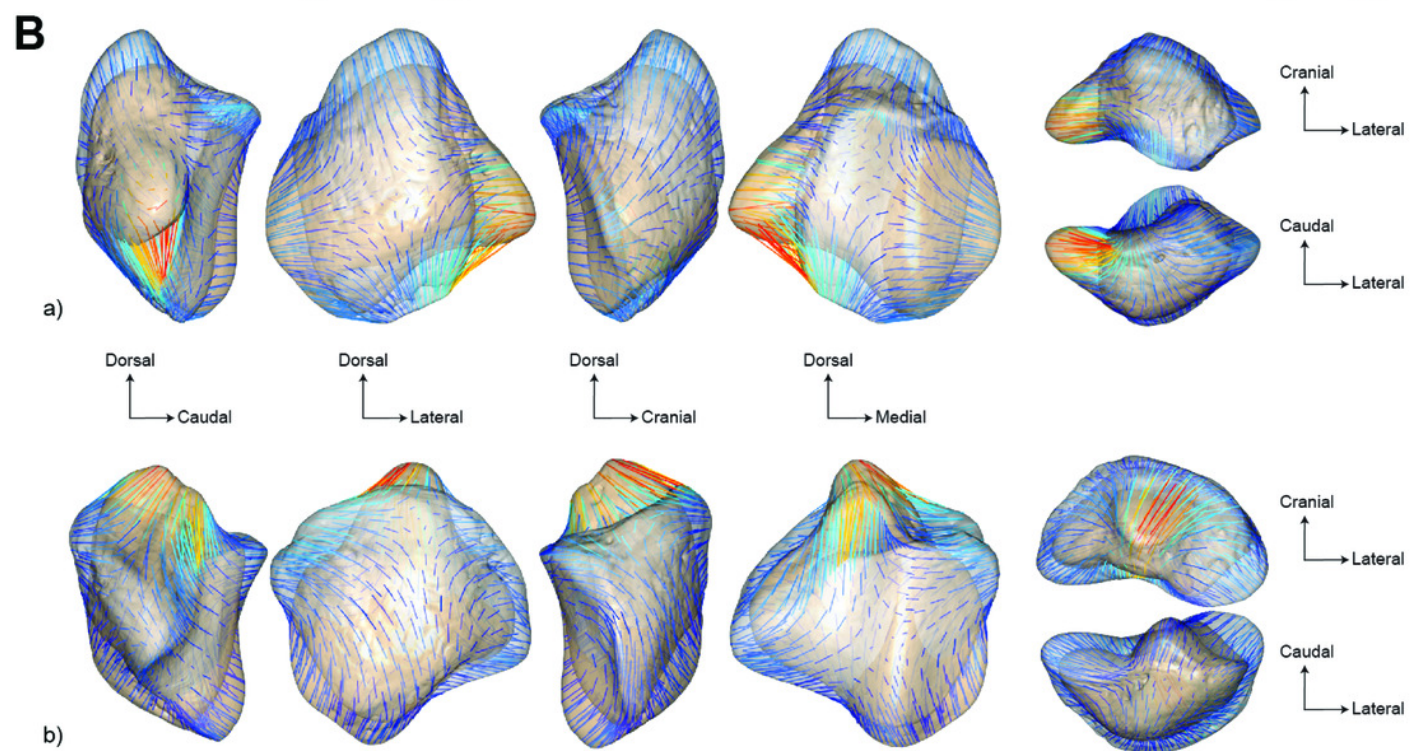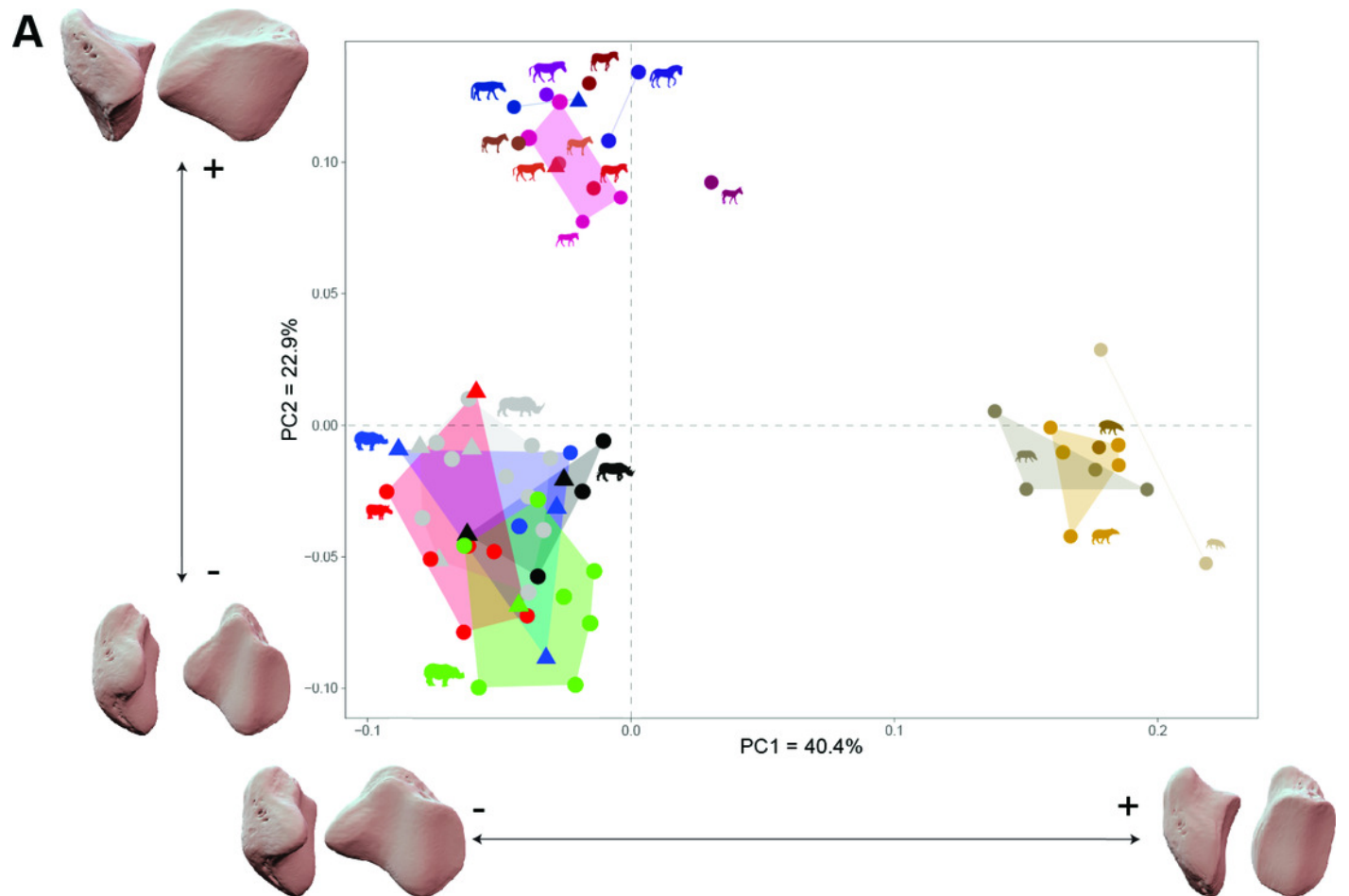
Figure 10

Results of the Procrustes ANOVA on shape data against log-transformed centroid size (CS) for all perissodactyls.

A: Regression plot with theoretical shapes associated with minimum and maximum fitted values (respectively in medial and caudal views). Colour code follows Figure 2. Point size is proportional to the mean log centroid size of each specimen **B:** Colour maps of the location and intensity of the shape deformation. The shape associated with the minimal CS value of the Procrustes ANOVA was coloured depending on its distance to the shape associated with the maximal value. Green indicates no deformation; blue indicates a negative deformation of high intensity; red indicates a positive deformation of high intensity.

A

B

Dorsal → Caudal

Dorsal → Lateral

Dorsal → Cranial

Dorsal → Medial

Cranial → Lateral

Caudal → Lateral

Direction and intensity of the shape variation

Negative — Positive
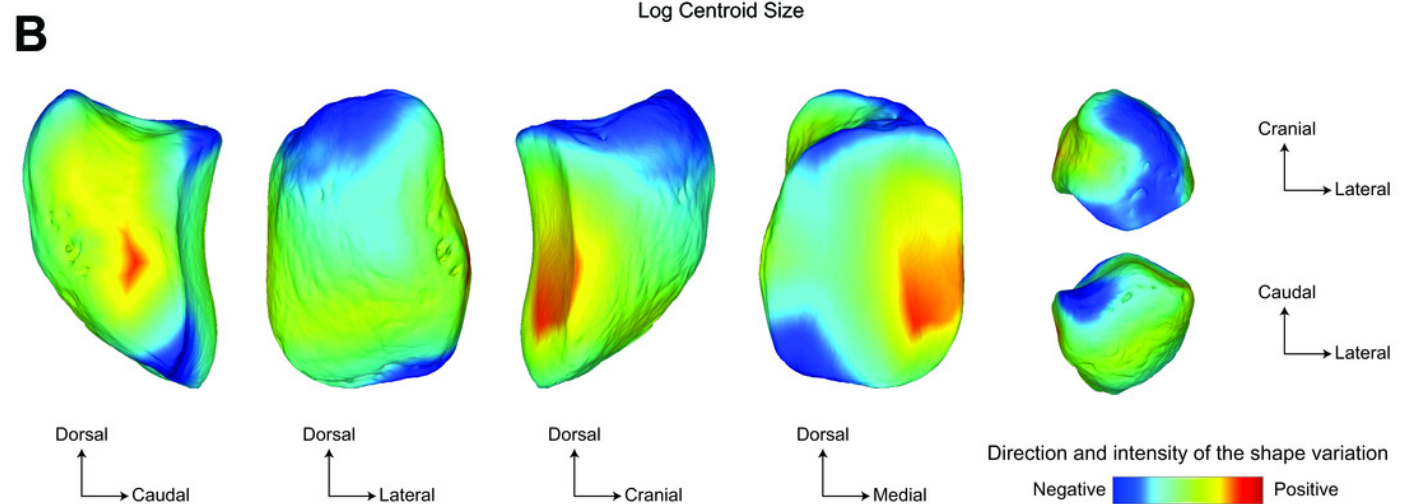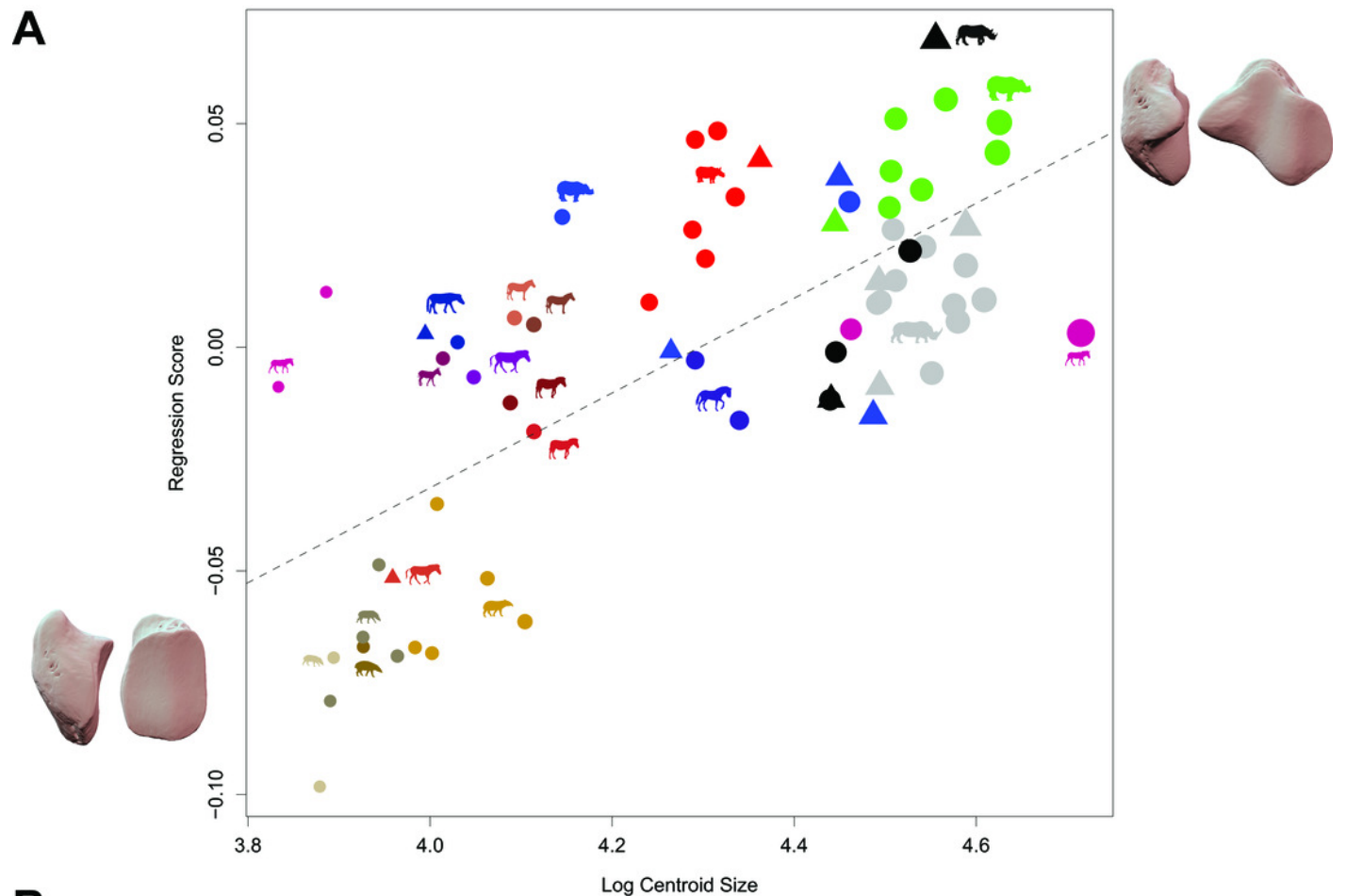
Table 1(on next page)

List of the studied specimens with family, genus and species names, mean body mass, institutions, sex, age class, condition, and 3D acquisition details.

Abbreviations: Sex: F: female; M: male; U: unknown. Age – A: adult; S: sub-adult. Condition – W: wild; C: captive; U: unknown. 3D acquisition – SS: surface scanner; P: photogrammetry; CT: CTscan. Stars indicate specimens retrieved on MorphoSource deposit. Institutional codes – AMNH: American Museum of Natural History. BICPC: Powell Cotton Museum, Birchington-on-Sea. IMNH: Idaho Museum of Natural History, Pocatello. MNHN: Muséum National d'Histoire Naturelle, Paris. MVZ: Museum of Vertebrate Zoology, Berkeley. NHMUK: Natural History Museum, London. NMB: Naturhistorisches Museum Basel, Basel. RBINS: Royal Belgian Institute of Natural Sciences, Brussels.

Family	Taxon	Mean body maSL (kg)	Institution	Collection number	Sex	Age	Condition	3D acquisition
Rhinocerotidae	*Ceratotherium simum*	2,300	AMNH	M-51854	F	A	W	SL
			AMNH	M-51855	M	A	W	SL
			AMNH	M-51857	F	A	W	SL
			AMNH	M-51858	M	A	W	SL
			AMNH	M-81815	U	A	U	SL
			BICPC	NH.CON.20	M	S	W	SL
			BICPC	NH.CON.32	F	S	W	SL
			BICPC	NH.CON.37	F	S	W	SL
			BICPC	NH.CON.110	M	A	W	SL
			BICPC	NH.CON.112	M	A	W	SL
			MNHN	ZM-MO-2005-297	M	A	C	CT
			NHMUK	ZD 1964.3.9.1	M	S	C	SL
			NHMUK	ZD 2018.143	U	A	U	SL
	Diceros bicornis	1,050	AMNH	M-27757	M	S	W	SL
			AMNH	M-113777	U	A	W	SL
			MNHN	ZM-AC-1936-644	F	S	U	SL
			MNHN	ZM-AC-1944-278	M	A	C	CT
			NHMUK	ZD 1879.9.26.6	U	U	U	CT
	Dicerorhinus sumatrensis	775	AMNH	M-81892	M	A	W	SL
			NHMUK	ZD 1879.6.14.2	M	A	W	SL
			NHMUK	ZD 1894.9.24.1	U	A	W	SL
			NHMUK	ZD 1931.5.28.1	M	S	W	SL
			NHMUK	ZE 1948.12.20.1	U	A	U	SL
			NHMUK	ZE 1949.1.11.1	U	A	W	SL
			NHMUK	ZD 2004.23	U	A	W	SL
	Rhinoceros sondaicus	1,350	MNHN	ZM-AC-A7970	U	A	U	SL
			NHMUK	ZD 1865.8.22.1	U	S	W	SL
			NHMUK	ZD 1871.12.29.7	M	A	W	SL
			NHMUK	ZD 1921.5.15.1	F	S	W	SL
			NHMUK	ZD 1861.3.11.1	U	S	W	SL
	Rhinoceros unicornis	2,000	AMNH	M-35759	M	A	C	SL
			AMNH	M-54454	F	A	W	SL
			AMNH	M-54456	F	U	S	SL
			MNHN	ZM-AC-1967-101	F	S	C	SL
			NHMUK	ZE 1953.8.13.2	F	S	U	SL
			NHMUK	ZE 1961.5.10.1	M	A	W	SL
			NHMUK	ZD 1972.822	U	A	U	SL
			NHMUK	ZD 1884.12.1.2	F	A	W	SL
Tapiridae	*Tapirus bairdii*	260	MVZ	141172	U	A	U	LS*
	Tapirus indicus	340	MNHN	ZM-AC-1931-528	M	A	C	CT
			MNHN	ZM-AC-1945-460	M	A	C	CT
			NMB	8125	F	A	C	CT
			RBINS	1184D	M	A	C	LS
			RBINS	1184E	M	A	C	LS

	Tapirus pinchaque	175	MNHN	ZM-AC-1982-34	M	A	C	CT
			MNHN	Indet	U	A	U	CT
	Tapirus terrestris	220	MNHN	ZM-AC-1937-1	U	A	C	CT
			MNHN	ZM-MO-1990-20	M	A	C	CT
			RBINS	1185D	M	A	C	LS
			RBINS	1185E	U	A	C	LS
Equidae	*Equus africanus asinus*	275	MNHN	ZM-AC-1893-634	M	A	C	CT
			MNHN	ZM-2005-717	U	A	U	CT
			RBINS	12970	F	A	C	LS
			RBINS	13076	F	A	C	LS
	Equus hemionus	230	MNHN	ZM-AC-1880-1103	M	A	C	CT
	Equus ferus caballus	490	MNHN	ZM-AC-A541	F	A	C	CT
			MVZ	162289	M	A	C	LS*
	Equus ferus przewalskii	250	MNHN	ZM-AC-1975-124	F	A	C	CT
			RBINS	14281	M	A	C	LS
	Equus burchellii granti	247	RBINS	33386	U	A	U	LS
	Equus grevyi	400	RBINS	32166	M	A	C	LS
	Equus quagga boehmi	247	RBINS	12129	M	A	W	LS
	Equus quagga chapmani	247	RBINS	1218	F	A	C	LS
	Equus quagga quagga	247	IMNH	R2425	U	A	U	LS*
	Equus zebra hartmannae	310	RBINS	3974	M	S	C	LS

1

Table 2**(on next page)**

Results of the Procrustes ANOVAs on shape data against log centroid size and femoral circumference respectively, and interaction with specific attribution, for adult rhinoceroses only.

Bold indicates results with a p value above 0.05 and considered as highly significant.

Abbreviations: dF: degrees of freedom; R²: coefficient of determination; F: F-statistics; Z: Z score; P: P value.

	dF	R^2	F	Z	P
Log Centroid size	1	**0.111**	**5.332**	**3.210**	**0.001**
Species	4	**0.437**	**5.247**	**5.368**	**0.001**
Interaction	4	0.076	0.917	-0.298	0.617
Residuals	18	0.375			
Log Femoral circumference	1	**0.107**	**5.135**	**3.088**	**0.001**
Species	4	**0.444**	**5.323**	**4.664**	**0.001**
Interaction	4	0.094	1.128	0.646	0.253
Residuals	17	0.355			

1

Table 3(on next page)

Results of the Procrustes ANOVAs on shape data against log centroid size and femoral circumference respectively, and interaction with specific attribution, for all perissodactyls.

Bold indicates results with a p value above 0.05 and considered as highly significant.

Abbreviations: dF: degrees of freedom; R^2: coefficient of determination; F: F-statistics; Z: Z score; P: P value.

	dF	R²	F	Z	P
Log Centroid size	1	**0.229**	**47.005**	**5.227**	**0.001**
Species	18	**0.554**	**6.305**	**10.043**	**0.001**
Interaction	10	0.046	0.944	-0.319	0.642
Residuals	35	0.171			
Log Femoral circumference	1	**0.253**	**52.401**	**5.454**	**0.001**
Species	18	**0.541**	**6.223**	**9.064**	**0.001**
Interaction	9	0.043	0.981	-0.911	0.533
Residuals	34	0.164			

1